Chapter 1

Introduction

The science that involves the study of friction, wear and lubrication of interacting surfaces in relative motion is known as Tribology. It mainly concerns with the basic need to minimize work and wear wherever loads and motion must be transmitted between two or more mechanical parts. It involves the modeling of lubrication phenomenon as well as the development of new lubricants and technologies for surface treatment. It deals with the optimization of tribological elements, to reduce the wear and power losses.

One of the major causes of wastage of material and loss in mechanical performance is the wearing out of components. Friction is one of the principal causes of wear and dissipation of energy. One of the most effective way of controlling friction and thus wear is lubrication. Most of the devices developed by mankind involve the interaction between surfaces and thus it wears out, most of the times because of relative motion between surfaces.

Though a lot of research has been done towards the design for the optimization of machinery components, wear, controlling friction between surfaces and lubrication is still a topic of intense research and development. A large amount of heat is being generated due to friction between the moving parts of a machine which results in power loss as well as change in working environment. About one third of global energy has been estimated to be spent in attempt to overcome friction in the various forms that it occurs. Clearly, there are potential economic benefits of reducing friction, and also the recent environmental concerns are responsible for the increasing interest in this field. Thus, Tribology can be described as a field of science which employs an operational analysis to problems of great economic significance, such as reliability, maintenance and wear of components.

Rotating machines are important assets in most of the industries. They constitute a fundamental unit for converting raw power into useful work. They are involved in almost every aspect of life, be it the crank shaft in the engine of an automobile, the hub on a bicycle, or the turbine/generator unit in a power plant. Regardless of their scale and use, all rotating machines usually have some sort of bearing which is used to separate the rotating part from the stationary part.

1.1 Bearings and its types

A bearing is machine element that constrains relative motion to solely the desired motion, and reduces friction between moving components. Bearing provides an easily sheared layer that allows the surface of the rotating part (shaft) to slide relative to the stationary part. The primary function of a bearing is to carry load and reduce the wearing out of material due to direct sliding contact between components.

There are numerous ways of classification of the bearings. However, one of the most common ways of classification of bearing is on the basis of type of frictional contact between the shaft and bearing. On the basis of type of frictional contact between shaft and bearing surface, bearing can be classified into two primary categories:

1. Sliding contact bearings
2. Sliding contact bearings.

1.1.1 Sliding Contact Bearings

Sliding Contact bearings have a surface of shaft which slides over the surface of bush thus causing wearing out and frictional losses. They are also called as plain bearings or journal bearings. A film of lubricating oil is provided between two surfaces which helps in separating the surface and thus minimize friction and wear. Based on the types of lubrication sliding contact bearings are further classified as Hydrodynamic Lubricated bearings and Hydrostatic lubricated bearings.

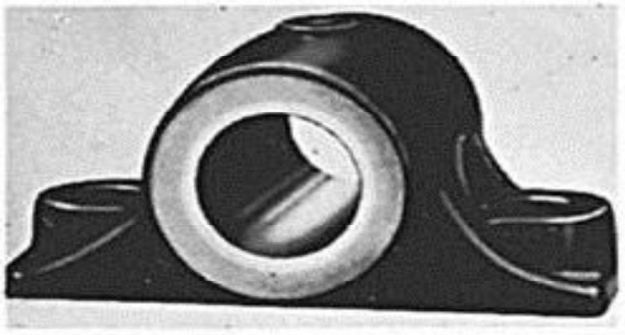

Figure 1.1 Sliding Contact Bearing [1]

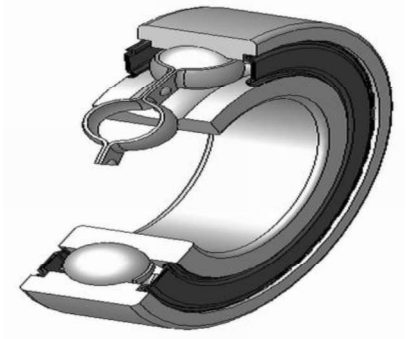

Figure 1.2 Rolling Contact Bearing [1]

1.1.2 Rolling Contact Bearings

Rolling contact bearings employs rolling elements like balls or rollers which transforms the sliding friction onto rolling friction. The rolling elements are placed between the two rings known as races. The inner race of the bearing remains in contact with the shaft while the rolling elements forms various point contacts with the outer race which is held stationary. The relative motion between the races causes the rolling elements to roll with very little rolling resistance and with little sliding. Rolling contact bearing can be further classified into various types as spherical roller bearings, cylindrical roller bearing, needle roller bearing etc.

1.1.3 Comparison between Sliding and Rolling Contact Bearing

Almost all heavy industrial turbo-machines use fluid film bearings of different types to support the shaft weight as well as control the disturbances and vibrations caused by unbalance forces. Fluid film bearings have following advantages over the rolling element bearings:

I. **Vibration Damping**: External or internal oscillations are quickly dampened in a well-designed journal bearing. The damping is vital in many rotating machines where the fluid film bearings are typically responsible for the absorption of excess of energy which is necessary to control vibrations.

II. **Fatigue Life**: In rolling contact bearings, rolling elements are in constant rolling motion in the raceway which results in metal fatigue. This fatigue generated is a typical cause of bearing failure. A journal bearing on the other hand has no metal-to-metal contact, so the theoretical fatigue life is extended. Journal bearings also have an incredibly long-life provided the lubricant is free from any contamination and supplied in appropriate quantity.

III. **Acoustical Performance**: In a ball bearing, a lot of noise is produced at high speeds because of the contact of balls with the raceway. Fluid film bearings, in contrast, are almost silent because of the presence of lubricant which prevents metal-to-metal contact.

IV. **Shock Performance**: An oil film separates the working parts of a fluid film bearing. The oil film acts as a shock absorber and prevents damage to the bearing surfaces.

1.2 Plain Bearings

Plain bearings are the simplest type of bearings in which there is only sliding contact between the mating parts and they do not possess any rolling element. Plain bearings can be further classified into three types:

- Radial bearings are the bearings which supports radial loads.
- Thrust bearings are the bearings which supports loads in axial direction.
- Guide or slipper bearings are the bearings which guides moving parts into a straight line.

Radial bearings also known as sleeve or journal bearings are the most commonly used type of plain bearings. These can be further classified into full journal bearing in which there is full 360° contact between mating parts and partial journal bearing in which there is less than 180° sliding contact between the mating parts.

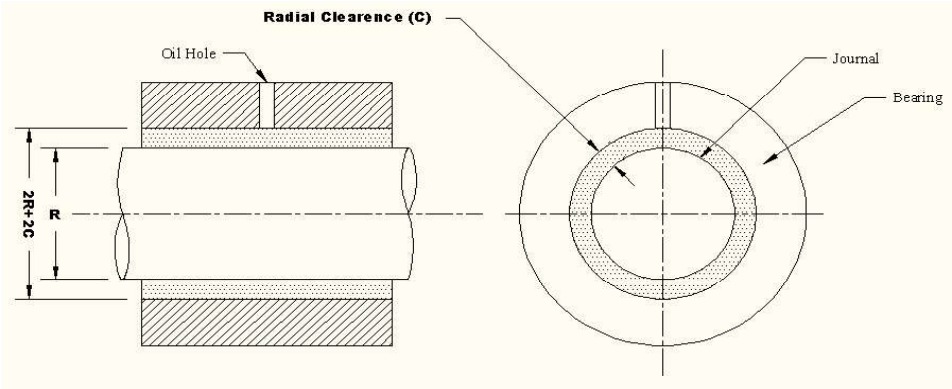

Figure 1.3 Full or 360° Journal Bearing

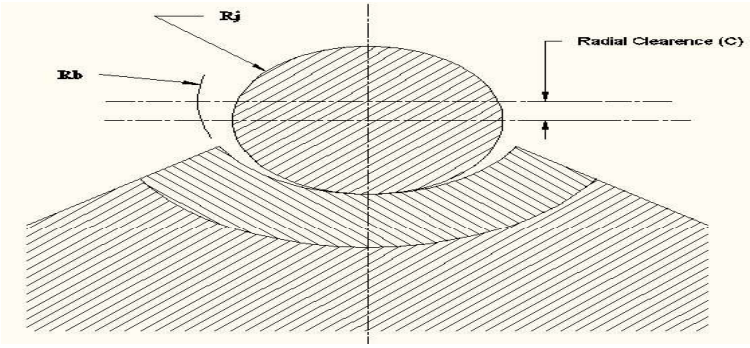

Figure 1.4 Partial journal bearing

1.3 Types of Lubrication

Lubrication is the science of reducing friction by application of a suitable substance called lubricant, between the rubbing surfaces of bodies having relative motion. The main aim of the use of a lubricant is to:

i. Reduce friction.

ii. Reduce or prevent wear and tear.

iii. Carry away heat generated due to friction.

iv. Protect against corrosion.

The basic modes of lubrication are thick and thin film lubrication.

1.3.1 Thin Film Lubrication:

Thin film lubrication or boundary lubrication corresponds to the condition when the film between the two surfaces in thin and a partial metal to metal contact is present between two surfaces. Boundary lubrication is generally seen under excessive load, insufficient surface area or oil supply, low speed and misalignment.

1.3.2 Thick Film Lubrication:

Thick film lubrication corresponds to a condition of lubrication, where two surfaces of bearing in relative motion are completely separated by a fluid film. The properties of surface have little or no influence on the performance of the bearing because of no contact between the surfaces. The resistance to the relative motion arises from the viscous resistance of the fluid. Therefore, the performance of the bearing is only affected by the viscosity of the lubricant. Thick film lubrication is further divided into two groups: hydrodynamic and hydrostatic lubrication.

Hydrodynamic Lubrication: Hydrodynamic lubrication can be defined as a system of lubrication in which the fluid film supporting the load is created by the relative motion and shape of the sliding surfaces. Hydrodynamic effect can be observed when two conditions are fulfilled. First condition being that the fluid film has a convergent-divergent geometry and the second condition being a relative motion between the shaft and the sleeve.

Hydrostatic Lubrication: Hydrostatic lubrication is defined as a system of lubrication in which the fluid film which supports the load and separates the two surfaces is created by an external source, like a pump, supplying sufficient fluid under pressure. Since the lubricant is supplied under pressure, this type of bearing is called externally pressurized bearing. Also it does not require the dynamic interaction between the surfaces in order to produce the lubricating effect.

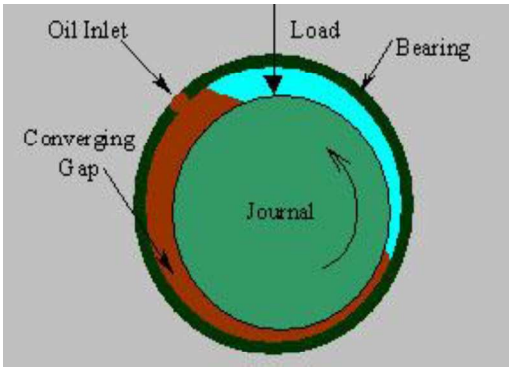

Figure 1.5 Hydrodynamic action in bearings [2]

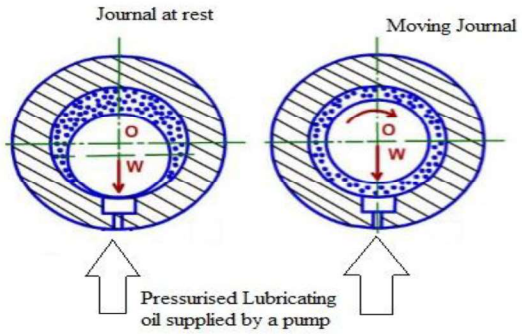

Figure 1.6 Hydrostatic action in bearings [2]

Stribeck curve is a graph between the coefficient of friction between the surfaces and the bearing modulus or bearing characteristic number, which is dependent on the lubricant viscosity, speed of rotation of the journal and the average pressure.

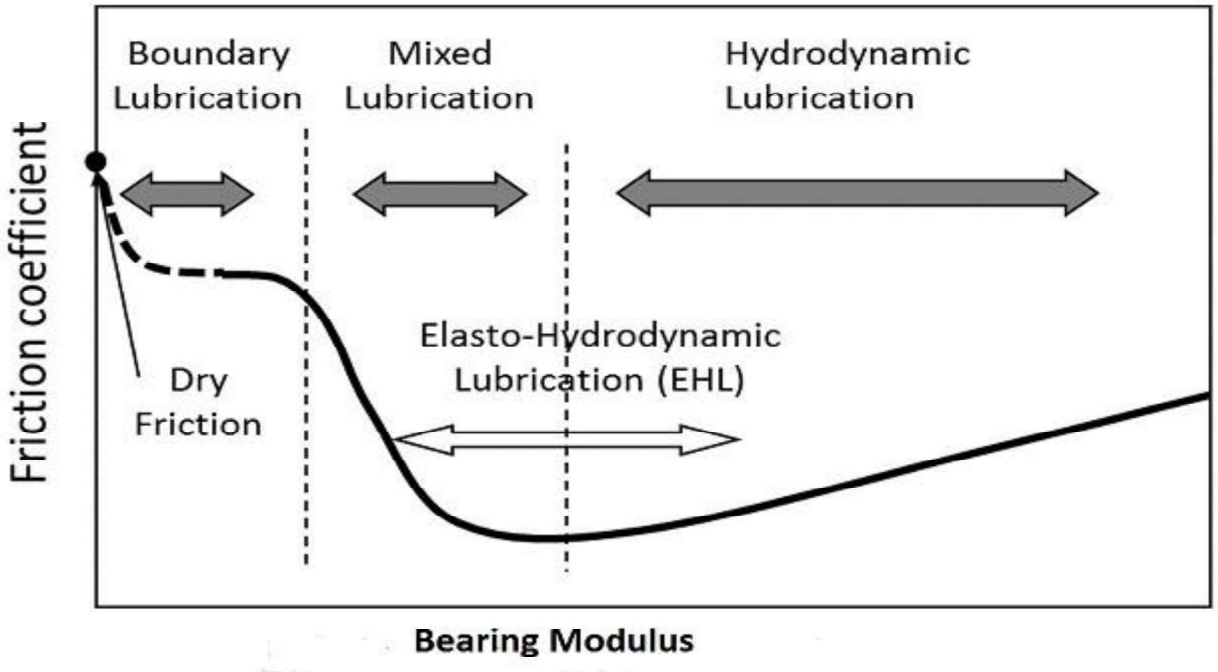

Figure1.7 Stribeck curve showing various regions of lubrication [3]

Stribeck curve divides the lubrication into three distinct zones. At rest, the two surfaces are in contact with each other and thus the coefficient of friction is quiet high. Lubricant pressure starts to build up with the onset of relative motion between the two surfaces. The load gets shifted from the asperities to lubricant because of pressure build up. With the building up of pressure in the lubricant the load shifts from the surface asperities to the lubricant. Further increase in speed or decreased in load or increase in lubricant viscosity, the bearing modulus keeps on increasing and thus the lubricant pressure continues to build, thus increasing the separation between the surfaces. With further increase of bearing modulus, lubricant pressure attains a value at which the surface are no more in contact and load is completely supported by the lubricant. A layer of lubricant is formed between the two surfaces which can be easily sheared off thus resulting in huge reduction of friction. With further increase in speed shear rate increases resulting in increased friction between surfaces. Wear of surfaces usually decreases as the lubrication regime changes from boundary lubrication to mixed lubrication and ideally there is no wearing out of surfaces in hydrodynamic lubrication regime.

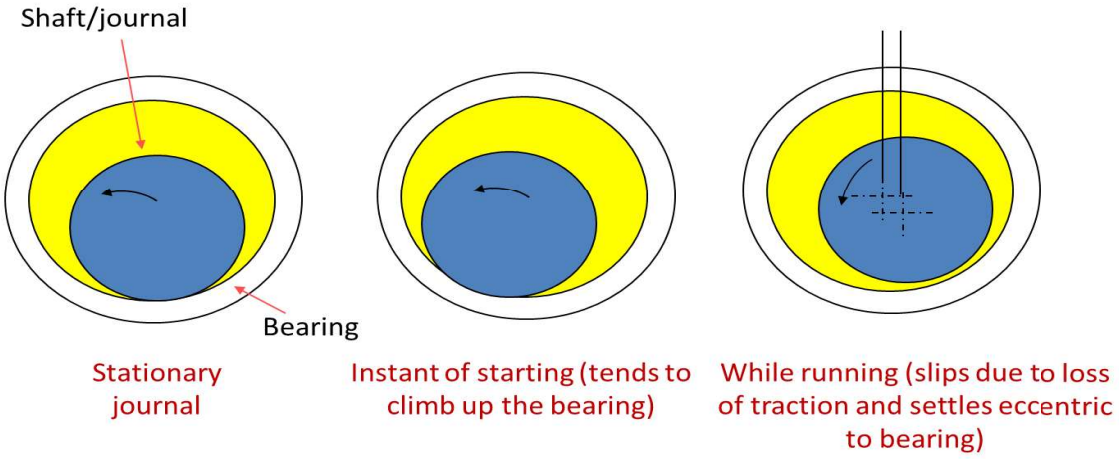

Figure 1.8 Hydrodynamic bearing in action [3]

Hydrodynamic journal bearing are one of the most widely used bearings with a large area of applications starting from mechanical components like pumps, compressors, fans, turbines etc. to even hard disks of computers. The characteristics of journal bearings depend on various mechanical and physical parameters like misalignment, shaft flexibility, load, temperature, etc. of the rotor-bearing system. Thus it is extremely important to consider all these parameters to predict the exact bearing characteristics.

1.4 Misalignment in journal bearings:

It has been found that most of the journal bearings operate under misalignment in normal conditions. However, independent designing is done for the shaft and journal bearing in any mechanism without the consideration of any interaction between them. However, it has been found that there is certainly interaction and interplays in shaft and bearing. The shaft gets deformed when a force (load) acts on it and it gets misaligned while in working condition.

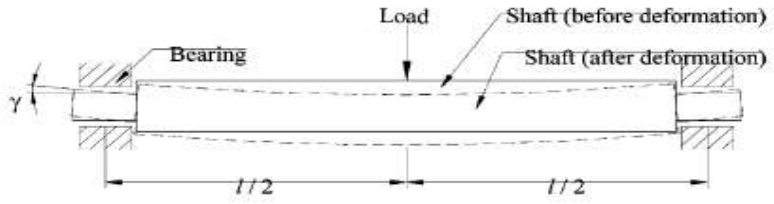

Figure 1.9 Misalignment produced due to loading [36]

The several reasons that might result in journal misalignment are:

- Thermal distortion of a shaft
- Deformation of a shaft due to heavy load
- Manufacturing errors
- Faulty bearing housing supports
- Improper installation
- Asymmetric load
- Wearing out of the shaft

Thus, it can be concluded that journal misalignment is an unavoidable error in the system and it is extremely important to consider the effect of this misalignment effect on the lubrication of a journal bearing.

Chapter 2

Literature Review

Journal bearing is a vast subject and it's has always been a hot topic for research and analysis. Exact analysis of journal bearings involves the study of a large number of factors affecting bearing performance and a lot of investigations have been done in this field. It is very difficult to include all the literature in this report; however a sincere effort has been made to bring about the literature which is closely related and available.

Journal bearings have been used since a long period of time but their lubrication principle was unknown until Reynolds equation was derived first by Reynolds [4] in 1886. Under certain assumptions Reynolds equation gave the relationship for the pressure of a convergent oil film in an eccentric journal bearing with the bearing parameters like lubricant viscosity, velocity and geometry. Since then a lot of investigations have been done by other researchers on Reynolds equation to obtain the pressure in an oil film.

Over the last few years, misalignment in journal as well as thrust bearings has been increasingly studied. Fisher [5] was one of the first researchers to notice the irregular heating of bearing as well as the differences in axial flow at bearing ends due to misalignment. The very first analysis on the misalignment of journal bearing was made by McKee et al. [6] which revealed the distribution of pressure in the axial direction. Piggott [7] showed that the load catrrying capacity of a bearing was reduced due to a misalignment of 0.0002 radians. However, in all of these studies misalignment only represented one part of work and was considered as a phenomenon which was limited to occur only in certain cases.

The first study that was completely dedicated to the concept of misalignment was carried out by Dubois et al. [8, 9 and 10] who studied the pressure field and the misalignment couple under journal misalignment. They observed increase in the maximum pressure and decline in the bearing performance because of the permanent deformation of the bearing at the ends. Smalley et al. [11] discussed in detail about the bearing misalignment of un-grooved bearings for different values of slenderness rations. Minimum film thickness and friction force of a two-groove bearing under misalignment in vertical plane was investigated by Asanable et al. [12].

Pinkus et al. [13] presented an in-depth analysis of misaligned bearings. They also presented some charts which depicted some important features of misaligned journal bearings. Mokhtar et al. [14] presented the solution for axially fed misaligned journal bearings considering adiabatic conditions. Buckholz et al. [15] studied the influence of misalignment on cavitation and load carrying capacity of journal bearings using non-Newtonian fluids. Jiang et al. [16] gave an adiabatic solution of a journal bearing under misalignment using non-Newtonian lubricants which obeys the power-law fluid model. A modified form of Elrod cavitation algorithm was used by Keith et al. [17] to study the consequences of misalignment on the performance of a journal bearing with a line groove for flooded as well as starved conditions.

Nicolas et al. [18] studied the changes in static as well as dynamic characteristics of hybrid bearings under the influence of misalignment of geometrical parameters for laminar as well as turbulent flow regimes and drew comparison between the experimental results and the results obtained from numerical procedures. Qiu et al. [19,20] investigated the characteristics of two misaligned journal bearings theoretically as well as experimentally. They studied and compared various static and dynamic characteristics for a grooved journal bearing with different value of eccentricities and misalignment conditions. An algorithm for the identification of damping and stiffness coefficients of a misaligned three lobe bearing was given by Arumugam et al. [21].

Banwait et al. [22] presented the thermo-hydrodynamic (THD) effects for circular plain journal bearings with misalignment. Guha [23] analyzed steady state performance characteristics of a misaligned journal bearing incorporating the effects of isotropic roughness, eccentricity ratio and degree of misalignment. Bouyer et al. [24] carried out an experiment to analyze the influence of misalignment on the performance of a plain journal bearing with a diameter of 100mm. Pierre et al. [25] developed a 3D thermo-hydrodynamic model for a misaligned plain journal bearings along with the consideration of thermal and cavitation effects. Booker et al. [26] investigated the transient as well as steady-state characteristics of groove-less misaligned bearings.

Ma [27] analyzed the performance characteristics for a dynamically loaded journal bearing with the incorporation of the consequences of couple stress and elasticity of the liner. Sun et al. [28] considered various parameters like thermal effects, surface roughness, the relationship between the viscosity and pressure of the lubricating oil and the deformation of the bearing surface to calculate the lubrication characteristics of a journal bearing under misalignment.

A steady state mixed TEHD thermo-elasto-hydrodynamic model was developed by Wang et al. [29] along with the consideration of fluid flow in the gap formed due to surface thermo-elastic deformations, rough surfaces, asperity contact and the angular misalignment between the bearing and journal. They also considered the variation of viscosity of lubricant with pressure and temperature. and the angular misalignment between the journal and the bearing. The model was further utilized to predict the importance of all these factors while analyzing mixed lubrication phenomenon for a journal bearing. Khonsari et al. [30] used a 3D thermo-hydrodynamic model with shaft temperature field to study the influence of misalignment on a journal bearing using a mass-conserving cavitation algorithm during analysis.

Ashour et al. [31] studied the pressure distribution, fluid film thickness and other bearing performance characteristics of a misaligned tilting-pad journal bearing under transient loading conditions using finite element analysis. Das et al. [32] carried out the study on the performance of misaligned journal bearing lubricated with micro-polar fluid under steady state. Papadopoulos et al. [33] presented a plot for the friction coefficient versus wear depths and misalignment angles for different values of Sommerfeld number. They also investigated the variation in loss of power for the rotor bearing system and obtained the power loss as a function of wear depth and misalignment angles. Pai et. al. [34] studied the effect of turbulence and misalignment on steady state characteristics of a centrally loaded single pad externally adjustable bearing using finite difference method to solve Reynolds equation.

Sun et. al. [35] analyzed the hydrodynamic lubrication characteristics of a journal bearing, taking in to consideration the misalignment caused by shaft deformation. Various parameters like film pressure, load-carrying capacity, attitude angle, end leakage flow-rate, frictional coefficient, and misalignment moment of a journal bearing were calculated for different values of misalignment degree and eccentricity ratio. Gui et. al. [36] developed a special test bench for the study on lubrication performance of cylindrical journal bearings. The effect of journal misalignment on oil film pressure, oil film thickness and oil temperature of journal bearing as a result of shaft bending under load was studied.

Xu et. al. [37] carried out a comprehensive analysis on the oil film pressure, oil film temperature, oil film thickness, load carrying capacity, oil film stiffness, and damping of journal bearing with different misalignment ratios considering the turbulent and thermo effects based on solving the

generalized Reynolds equation and energy equation. Jang et. al. [38] reviewed the effect of misalignment on the static and dynamic performances. They presented the basic theory for the misalignment and presented some results for the circular journal bearing to show the general trends of the misalignment.

Scientists have been involved in predicting the effect of misalignment in journal bearings. Also it has been tried to rectify the problem arising from it. Still there is need of further research for investigating the accurate effect of the misalignment in the journal bearings. Modern techniques and tools have facilitated the researchers in the modelling and simulation of exact and real world problems. Also the defects and results with the current scenario must be rectified for further investigations.

In this project, an effort has been made to understand the behaviour of a journal bearing under the misaligned conditions. A numerical approach has been used which is based on finite difference method in order to get the operational characteristics of the bearing.

Chapter 3

Calculation of the characteristics of journal bearings

3.1 Journal Bearings

Journal bearings are very common engineering components and are used in almost all types of machinery. Combustion engines and turbines virtually depend on journal bearings to obtain high efficiency and reliability. Journal bearing is a type of bearing having a plain surface to support the load and uses a lubricant which helps in reducing the friction between the rotating and the stationary part. These types of bearings are also termed as fluid film bearings because of the presence of a film of lubricant between shaft and bearing. It consists of a shaft rotating within a stationary bush.

3.1.1 Bearing Geometry

A journal bearing consists of a journal which is attached to the shaft using some key and it rotates along with the shaft inside a stationary bush. A lubricant is provided in between the bearing and the journal which supports the load by the formation of a film. A journal bearing in operation has been depicted in figure 3.1. Some of the important parameters of a journal bearing geometry are:

I. **Radial clearance (c)**: Radial clearance refers to the clearance along the radius of a bearing and a journal. It is given by the difference of the radii of the bearing and journal. Mathematically it is given as

$$c = R_2 - R_1$$

The radial clearance (c) in a bearing should be small enough to produce the necessary velocity gradient, so that the pressure built up in the lubricant can support the load. Small clearance also helps in reducing the flow rate due to side leakage in bearings. However, the allowance must be made for manufacturing tolerances in the journal and bushing.

II. **Eccentricity (e):** During operation of a journal bearing, the journal rotates with a center different from the center of bearing. The radial distance between these centers is known as eccentricity.

III. **Clearance ratio:** It is defined as the ratio of radial clearance between bearing and journal to the radius of journal.

IV. **Attitude or Eccentricity ratio:** It is defined as the ratio of eccentricity (defined in point II) to radial clearance between the bearing and journal (defined in point I)

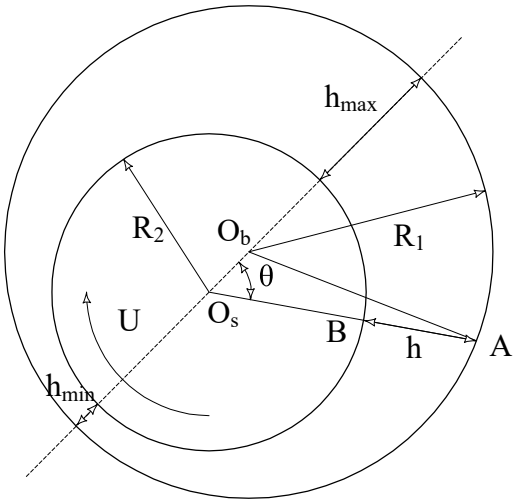

Figure 3.1 Journal bearing geometry where O_b and O_s are centers of bearing and shaft respectively, R_1 and R_2 is the radius of bearing and journal respectively, h is the film thickness

V. **Minimum thickness of Oil film (h_{min}):** It is the minimum thickness of the lubricating oil film when the bearing is under operation. It is given by the minimum radial distance between journal and bearing and it occurs along the center line.

VI. **Attitude Angle (φ)**: It is the angle between the line of centers and the direction of loading in the bearing.

Now, considering the triangle O_sO_bAB (figure 3.2) from the journal bearing geometry, for small angle of inclination (α) it can be written as

$$O_sA = O_sC + CA = O_sB + BA$$

or $$O_sA = ecos\theta + R_1cos\alpha = R_2 + h$$

thus $$h = ecos\theta + R_1cos\alpha - R_2$$

On the further simplification of the equation using sine rule it can be written as

$$h = ecos\theta + R_1 - R_2 = ecos\theta + c$$

or $$h = \varepsilon(1 + cos\theta) \qquad (3.1)$$

where ε is the eccentricity ratio.

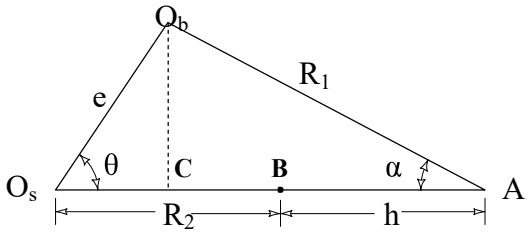

Figure 3.2 Part of journal bearing geometry, e is the eccentricity between journal and bearing, α is the inclination angle or wedge angle

3.2 Reynolds Equation and Journal bearings

The mechanism of hydrodynamic lubrication can be described by Reynolds equation. It was given by Osborne Reynolds and is a general equation that analyses different types of hydrodynamic lubrication. Hydrodynamic lubrication is defined as the occurrence of relative motion between two surfaces which causes fluid to form a lubricating wedge. Reynolds equation is a combined equation formed using Navier-stokes and continuity equation.

For the hydrodynamic lubrication to take place, there are two necessary things:

I. Relative motion with sufficient velocity for film formation.
II. Inclination of surface as some angle for pressure generation.

The principle of pressure generation in hydrodynamic lubrication between two moving inclined surfaces can be schematically illustrated as in figure 3.3.

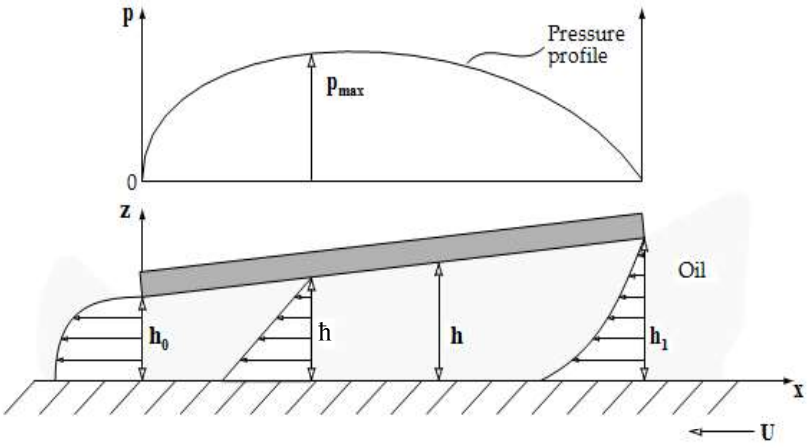

Figure 3.3 Principle of hydrodynamic pressure generation [45]

As the bottom surface starts rotating, lubricant is dragged by it along with itself. However the upper plate being inclined to the lower plate results in an increase in pressure of lubricant, which

results in formation of a pressure field. At the beginning of the wedge, the pressure goes on increasing which restricts the entry of lubricant. The pressure reaches its maximum value and then it starts to decrease thus boosting the exit flow. Thus the fluid velocity profile is bend inwards at the entrance and bend outwards at exit because of the pressure gradient as depicted in Figure 3.3. As a result, the two surfaces are separated by the pressure generated by the wedging action and it is also able to support a certain load. The formation of planar wedge around a shaft results in pad bearings, while a curved or wrapped wedge results in journal bearings.

In order to understand the mathematical description of the fundamental mechanism underlying hydrodynamic lubrication, certain assumptions are to be made. All the simplifying assumptions necessary for the derivation of the Reynolds equation are summarized in Table 3.1.

	Assumption	Comments
1	Body forces are neglected	Always valid, since there are no extra outside fields of forces acting on the fluids with an exception of magneto-hydrodynamic fluids and their applications.
2	Pressure is constant through the film	Always valid, since the thickness of hydrodynamic films is in the range of several micrometers. There
3	No slip at the boundaries	Always valid, since the velocity of the oil layer adjacent to the boundary is the same as that of the
4	Lubricant behaves as a Newtonian fluid	Usually valid with certain exceptions, e.g. polymeric oils.
5	Flow is laminar	Usually valid, except large bearings, e.g. turbines.
6	Fluid inertia is neglected	Valid for low bearing speeds or high loads. Inertia effects are included in more exact analyses.
7	Fluid density is constant	Usually valid for fluids when there is not much thermal expansion. Definitely not valid for gases.
8	Viscosity is constant throughout the generated fluid film	Crude assumption but necessary to simplify the calculations, although it is not true. Viscosity is not constant throughout the generated film.

Table 3.1 Assumptions made in Reynolds equation

Reynolds equation can be obtained by combining the Newton's second law of motion and continuity equation for the lubricant between the shaft and the bearing. Reynolds equation in three dimensions can be given as in equation 3.1.

$$\frac{\partial}{\partial x}\frac{(h^3)}{\eta}\frac{\partial p}{\partial x} + \frac{\partial}{\partial y}\frac{(h^3)}{\eta}\frac{\partial p}{\partial y} = 6\left(U\frac{dh}{dx} + V\frac{dh}{dy}\right) + 12(w_h - w_o) \qquad (3.2)$$

where, u, v and w represents the velocities along x, y and z axis respectively, h represents thickness of the wedge, η represents absolute viscosity of the lubricant and p depicts the pressure.

Bearing parameters predicted by Reynolds Equation

Majority of the important critical design parameters of bearings can be obtained by the simple integration of Reynolds equation. These parameters are:

I. **Pressure Distribution**: Pressure distribution for a bearing is obtained by the integration of Reynolds equation over a specified fluid film h=f(x,y).

II. **Load Capacity**: The load carrying capacity of a bearing is by the integrating the pressure distribution of the bearing obtained previously over the corresponding area of cross section. For change in load, the bearing film geometry changes and thus the pressure field also changes. The load that can be supported by a bearing for a particular film geometry is given as

$$W = \int_0^L \int_0^B p.dx.dy \qquad (3.3)$$

However, in journal bearings the fluid film formed between the shaft and the bearing surface is initially converging, reaches a minimum thickness and then starts diverging again. The pressure increases in the converging area while it decreases in the diverging area. This leads to the formation of negative pressure in the diverging area. Also the load carrying capacity of bearing comes out to zero because of the symmetrical distribution of positive and negative pressure over the bearing halves. Also negative pressure formation is impossible in a bearing. The negative pressures results in cavitation in the fluid film. Also, Half-Sommerfeld conditions are commonly used for load calculations, i.e. the negative pressures in one half of the bearing are discounted.

Load was calculated from two components, one acting along the line of shaft and bush centres and a second component perpendicular to the first. The attitude angle

can be calculated through this method. The pressure distribution and load components for a journal bearing have been depicted in Figure 3.4.

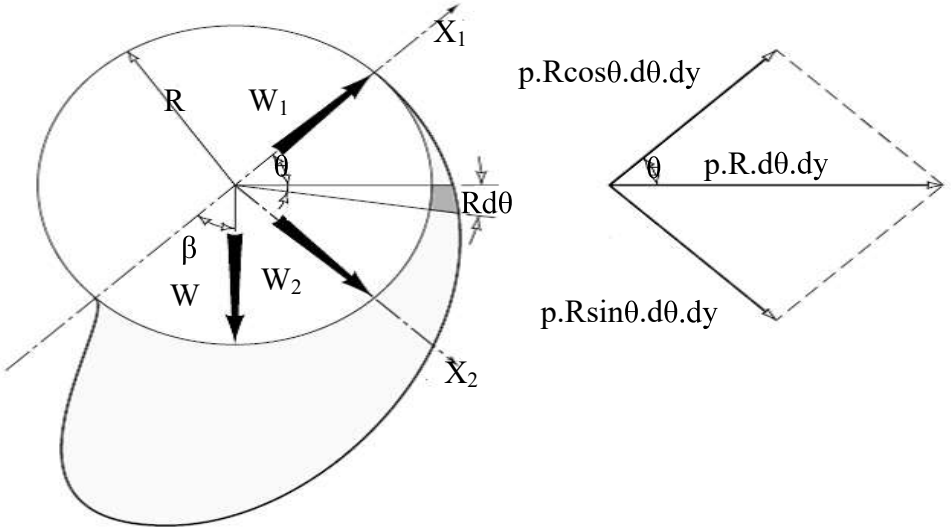

Figure 3.4 Pressure field and load components in a journal bearing

To obtain the expressions of the load components W_1 and W_2, a small element of area R.dθ.dy is considered. A plane surface can be obtained as the film of the journal bearing is unwrapped as shown in figure 3.5. It is similar to the formation of cylinder due to rolling of a sheet. This view gives a complete visualization of the film.

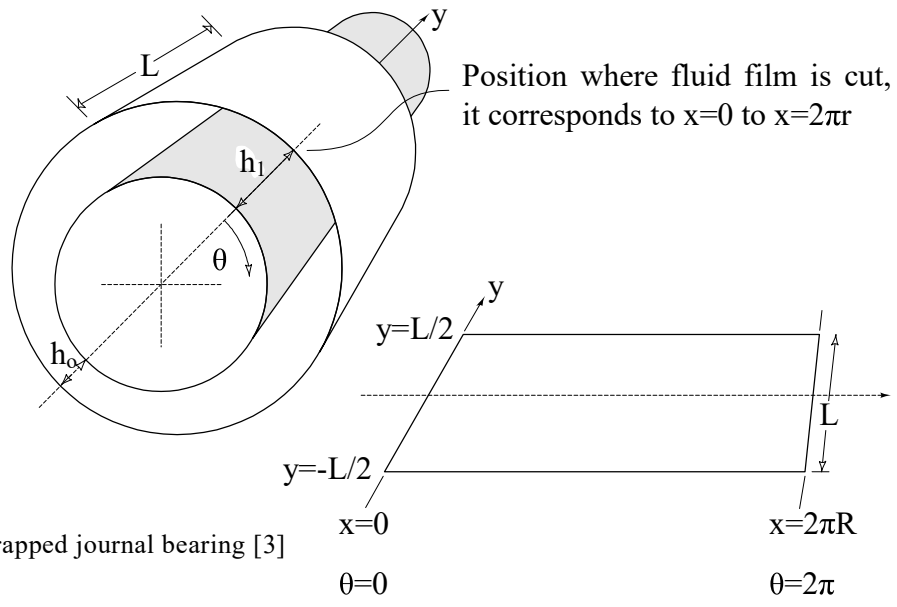

Figure 3.5 Unwrapped journal bearing [3]

For the small element considered, the incremental force exerted due to hydrodynamic pressure can be resolved into two components:

- p.Rcosθ.dθ.dy which acts along the line joining bush and shaft centres.
- P.Rsinθ.dθ.dy which acts normal to the line joining centres.

Thus the load component along the line of centres can be given as:

$$W_1 = \int_0^{\pi} \int_{-L/2}^{L/2} p.Rcos\theta.d\theta.dy \qquad (3.3)$$

Similarly, the load component in the normal direction can be given as:

$$W_2 = \int_0^{\pi} \int_{-L/2}^{L/2} p.Rsin\theta.d\theta.dy \qquad (3.4)$$

The total load supported by the bearing can be expressed as:

$$W = \sqrt{W_1^2 + W_2^2} \qquad (3.5)$$

III. **Sommerfeld Number:** Sommerfeld number or duty parameter is an important parameter for journal bearings as it can express the load carried by the bearing as a function of eccentricity ratio. It can be expressed as in equation (3.6).

$$S = \frac{\eta N}{p}\left(\frac{R}{c}\right)^2 \qquad (3.6)$$

where p refers to the pressure calculated over the projected area of the film.

IV. **Friction Force**: Under the assumption that the only shear stress is caused due to friction force, it can be obtained by the integration of shear stresses over the whole bearing area.

$$F = \int_0^L \int_0^B \tau.dx.dy \qquad (3.7)$$

Shear stress at any point in the fluid film can be expressed as

$$\tau = \eta\frac{du}{dz}$$

where du/dz is the velocity gradient.

V. **Coefficient of friction**: The coefficient of friction can be obtained as the ratio of load and the friction force, which have been obtained previously.

$$\mu = \frac{F}{W} = \frac{\int_0^L \int_0^B \tau.dx.dy}{\int_0^L \int_0^B p.dx.dy} \qquad (3.8)$$

The virtue of hydrodynamic analysis is that it is concise, simple, and the same procedure can be applied to different kinds of bearing geometries whether its linear bearing or journal bearing or step bearing. With the introduction of effects like misalignment, heating, variation in local

viscosity, elastic deformation, cavitation etc the solutions become complex. However, the basic method of analysis remains unchanged.

3.3 Practical and operation aspects of journal bearing

Journal bearings are commonly incorporated as integral parts of various machineries with a wide range of design requirements. Thus there are some problems associated with practical implementation and operation of journal bearings. For example, in many practical applications the lubricant is fed under pressure into the bearing or there are some critical resonant shaft speeds to be avoided. The shaft is usually misaligned and there are almost always some effects of cavitation for liquid lubricants. Elastic deformation of the bearing will certainly occur but this is usually less significant than for pad bearings. All of these issues will affect the performance of a bearing to some extent and allowance should be made during the design and operation of the bearing. Some of the major issues affecting journal bearing performance have been discussed in the following sections.

I. **Misalignment:** In most of the practical applications, the axis of shaft is not aligned parallel to the bearing axis. Even if the shaft is accurately aligned during assembly, the load on the shaft causes bending and tilting of the shaft in a bearing. The critical minimum film thickness will occur at the edge of the bearing, as shown in Figure 3.6. The critical film thickness for misaligned shafts thus gets considerably lesser than for parallel shafts. The basic parameter to describe the misalignment of the shaft is the misalignment factor or tilt ratio which is defined as:

$$t = \frac{m}{c} \tag{3.9}$$

where t refers to the tilt ratio

m refers to the distance between axes of misaligned shaft and bearing axis measured at the edge

c refers to the radial clearance

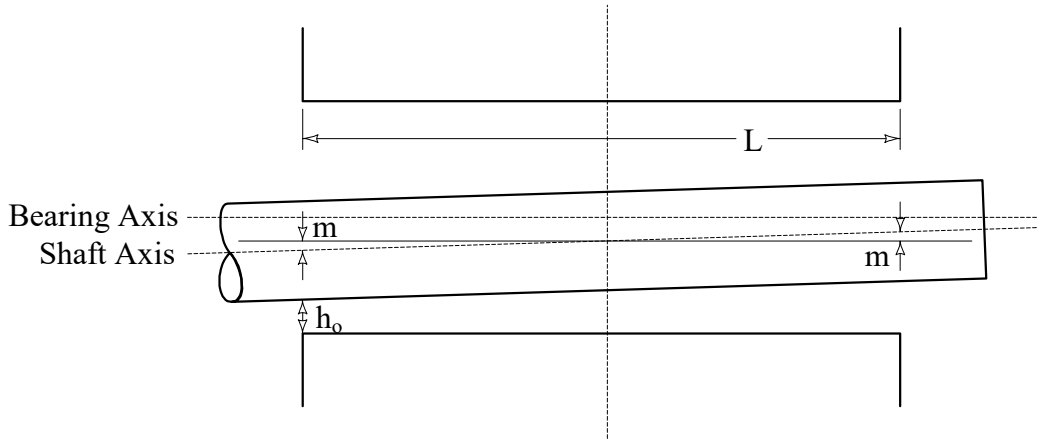

Figure 3.6 Details of misalignment in journal bearing

The minimum film thickness reduces due to misalignment. Assuming that minimum film thickness occurs along the load line it is given by the equation (3.10)

$$h_o = c(1 - cos\beta) - m \qquad (3.10)$$

where β refers to the attitude angle

In most cases of heavily loaded shafts, the attitude angle is small and its cosine can be approximated by unity.

To calculate the effect of misalignment on bearing geometry, the Reynolds equation is applied to the journal bearing with a film geometry modified by misalignment. The various parameters for the journal bearing may change due to the change in film thickness equation.

II. **Oil whirl or vibration caused by lubricant:** Oil whirl is the colloquial term describing hydro-dynamically induced vibration of a journal bearing. It can cause severe problems in the operation of journal bearings and thus it should be considered during the design process. Oil whirl is characterized by severe vibration of the shaft which occurs at a specific speed. Another form of bearing vibration known as 'shaft whip' is caused by the combined action of shaft flexibility and bearing vibration characteristics.

Although it may appear unlikely that a liquid such as oil would cause vibration, but as per the hydrodynamic theory, a change in load on the bearing is always accompanied by a finite displacement. This constitutes a form of mechanical stiffness or spring constant and when combined with the mass of the shaft, vibration is the natural result. A rotating shaft

nearly always provides sufficient exciting force due to small imbalance forces. It is essential to know the critical speed at which oil whirl occurs and avoid it during operation. It has been found that severe whirl occurs when the shaft speed is approximately twice the bearing critical frequency [].

A complete analysis of bearing vibration is quiet complex as it involves non-linear stiffness and damping coefficients. However a simple means of determining the occurrence of unstable vibration is based on linearized stiffness and damping coefficients. These coefficients are accurate for small stable vibrations and a critical shaft speed is found by this method.

Factors such as grooves, misalignment and elastic deformation have a strong (usually negative) influence on vibrational stability and are the subject of continuing study. Large angular extent grooves, e.g. 90° extent, are particularly deleterious to stability.

One of the most accepted solutions of bearing vibration problems is to apply specially designed bearings with an anti-whirl configuration. It is based on the basic principle of destroying the symmetry of a plain journal bearing which encourages vibration. Although many anti-whirl configurations have been patented no solution has yet been found that completely eliminates oil whirl.

III. **Cavitation:** As discussed previously, large negative pressures in the hydrodynamic film are predicted when surfaces move apart or mutually sliding surfaces move in a divergent direction. However, for most liquids a phenomenon known as cavitation occurs when the pressure falls below atmospheric pressure.

The reason for this is that most liquids contain dissolved air and minute dirt particles. When the pressure becomes sub-atmospheric, bubbles of previously dissolved air nucleate on pits, cracks and other surface irregularities on the sliding surfaces and also on dirt particles. It has been shown that very clean fluids containing a minimum of dissolved gas can support negative pressures but this has limited relevance to lubricants which are usually rich in wear particles and are regularly aerated by churning.

If there is a significant drop in pressure, the operating temperature can be sufficient for the lubricant to evaporate. The lubricant vapour accumulates in the bubbles and their sudden collapse is the cause of most cavitation damage. When a bubble collapses against a solid surface very high stresses are generated and this will usually cause wear. Wear

caused by cavitation progressively damages the bearing until it ceases to function effectively. The risk of occurrence of cavitation increases the elevation of bearing speeds and loads. Cavitation in bearings is also referred to as ‘film rupture’.

Large lubricant supply grooves have been found to suppress negative hydrodynamic film pressures and so prevent cavitation. This practice is similar to using partial arc bearings and has the disadvantage of raising the lubricant flow rate and the precise location of the cavitation front varies with eccentricity. This means that cavitation might only be prevented for a restricted range of loads and speeds. In practice it is very difficult to avoid cavitation completely with the conventional journal bearing.

Various other factors like lubricant supply, grooving in journal bearings, elastic deformation of bearings, movable pads, partial bearings etc. affects the operational characteristics of a journal bearing. However, this project report has been limited to the prediction of effect of misalignment of bearing on the operational characteristics and vibrational stability of bearings.

Chapter 4

Computational Approach for Journal Bearing

The differential equations which arose from the Reynolds equation and other theories were complex and can't be solved by analytical methods. Many efforts were made to work out on these equations using specialized and obscure mathematical functions, but these processes were tedious and the reach of solutions was limited. A gap or discrepancy always existed between what was needed in the engineering solutions to hydrodynamic problems and the solutions available. Analogue methods like electrically conductive paper were used as the means of determining the hydrodynamic pressure fields. However, with the development of numerical techniques to solve differential equations these methods became largely obsolete. These changes radically affected the general understanding and approach to various fields like hydrodynamic lubrication, heat transfer etc.

This chapter deals with the application of numerical techniques to the phenomenon of hydrodynamic lubrication. 'Finite Difference Method' has been used to understand the basic process.

4.1 Non-dimensionalization of the Reynolds equation

Non- dimensionalization refers to the technique of substituting all the real variables is an equation with the dimensionless fraction of two or more parameters. It helps in the generalization of a numerical solution. One of the basic disadvantages of a numerical solution is that the data is provided only for specific values of controlling variables. On the other hand, analytical expressions are not limited to any specific values and are suited for providing data for general use. In order to provide a comprehensive coverage of all the controlling parameters, a computer program has to be executed several times for different cases. Non-dimensionalization helps in reducing the controlling parameters and thus required information can be obtained from limited set of data.

The Reynolds equation (3.1) has been expressed in terms of film thickness 'h', pressure 'p', entraining velocity 'U' and dynamic viscosity 'η'. Non-dimensional forms of the equation's variables are following:

$$h^* = \frac{h}{c}\ ; x^* = \frac{x}{R}\ ;\ y^* = \frac{y}{L}\ ;\ p^* = \frac{pc^2}{6URη} \tag{4.1}$$

where ‘h’ is the hydrodynamic film thickness [in m]

‘c’ is the bearing radial clearance [in m]

‘R’ is the bearing radius [in m]

‘L’ is the bearing axial length [in m]

‘p’ is the pressure [in Pa]

‘U’ is the bearing entraining velocity [in m/s]

‘η’ is the dynamic viscosity of the lubricant [in Pa-s]

x, y are hydrodynamic film coordinates

The Reynolds equation in the non-dimensional form is given as:

$$\frac{\partial}{\partial x}\left(h^{*3}\frac{\partial p^*}{\partial x^*}\right) + \left(\frac{R}{L}\right)^2\frac{\partial}{\partial y}\left(h^{*3}\frac{\partial p^*}{\partial y^*}\right) = \frac{\partial h^*}{\partial x^*} \tag{4.2}$$

4.2 The Vogelpohl parameter

In 1930’s Vogelphal parameter was developed to improve the accuracy of numerical solutions using Reynolds equation [ ]. It is denoted by ‘M_v’ and is defined in equation 4.3.

$$M_v = p^* h^{*1.5} \tag{4.3}$$

On the substitution of the above parameter is the non-dimensional form of Reynolds equation, it is obtained as the equation 4.4.

$$\frac{\partial^2 M_v}{\partial x^2} + \left(\frac{R}{L}\right)^2\frac{\partial^2 M_v}{\partial y^2} = FM_v + G \tag{4.4}$$

where the parameter ‘F’ and ‘G’ can be defined as

$$F = \frac{0.75\left[\left(\frac{\partial h^*}{\partial x^*}\right)^2 + \left(\frac{R}{L}\right)^2\left(\frac{\partial h^*}{\partial y^*}\right)^2\right]}{h^{*2}} + \frac{1.5\left[\frac{\partial^2 h^*}{\partial x^{*2}} + \left(\frac{R}{L}\right)^2\frac{\partial^2 h^*}{\partial y^{*2}}\right]}{h^*} \tag{4.5}$$

$$G = \frac{\frac{\partial h^*}{\partial x^*}}{h^{*1.5}} \tag{4.6}$$

The Vogelpohl parameter facilitates computing by simplifying the differential operators of the Reynolds equation, and furthermore it does not show high values of higher derivatives in the final solution, i.e. d^nM_v /dx^{*n} where n > 2, unlike the dimensionless pressure 'p*'. This is because, where there is a sharp increase in 'p*' close to the minimum of hydrodynamic film thickness 'h*', 'M_v' remains at moderate values. Large values of higher derivatives cause significant truncation error in numerical analysis.

4.3 Finite difference approximation in Reynolds equation

Finite difference method has been used for journal bearing analysis. It is based on approximating a differential quantity by the difference between function values at two or more adjacent nodes. For example, the finite difference approximation to $\partial M_v/\partial x^*$ is given by:

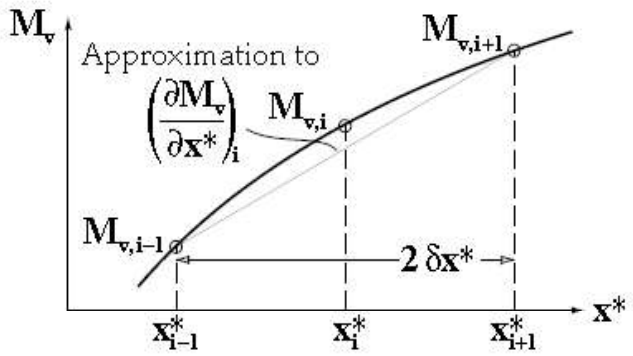

Figure 4.1 Approximation using Finite Difference Method [41]

$$\frac{\partial M_v}{\partial x^*} \approx \frac{M_{v,i+1} - M_{v,i-1}}{2\delta x^*} \tag{4.7}$$

where the subscript i+1 and i-1 denote the position immediately just behind and in front of the central position 'i' and δx* refers to the length of steps between the nodes.

Similarly, the expression for $\partial^2M_v/\partial x^{*2}$ can be found by subtracting the expression for $\partial M_v/\partial x^*$ at node i-0.5 from the i+0.5 nodal position and dividing by δx^*.

$$\left(\frac{\partial^2 M_v}{\partial x^{*2}}\right)_i \approx \frac{(\frac{\partial M_v}{\partial x^*})_{i+0.5} - (\frac{\partial M_v}{\partial x^*})_{i-0.5}}{\delta x*} \tag{4.8}$$

Also, it can be given as

$$(\frac{\partial M_v}{\partial x^*})_{i+0.5} \approx \frac{M_{v,i+1} - M_{v,i}}{\delta x^*}$$

$$(\frac{\partial M_v}{\partial x^*})_{i-0.5} \approx \frac{M_{v,i} - M_{v,i-1}}{\delta x^*}$$

Substituting these expressions in equation 5.2, results in

$$\left(\frac{\partial^2 M_v}{\partial x^{*2}}\right)_i \approx \frac{M_{v,i+1} + M_{v,i-1} - 2M_{v,i}}{\delta x^{*2}} \tag{4.9}$$

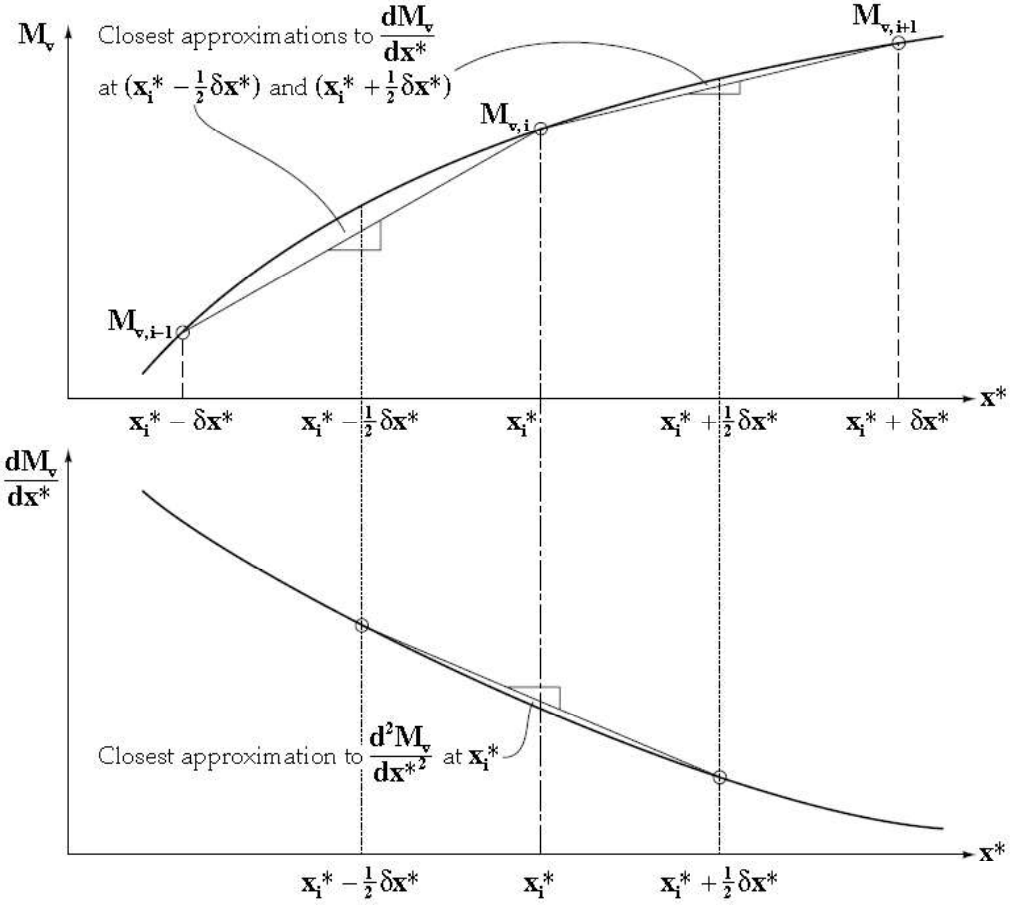

Figure 4.2 Principle for the derivation of finite difference approximation of second derivative of a function [41]

Similarly, the expression for ($\partial^2 M_v / \partial x^{*2} + \partial^2 M_v / \partial y^{*2}$) is calculated using finite difference variation of M_v along 'x' and 'y' axes. 'j' parameter is introduced as a second order nodal

variable along the 'y' axis. The coefficients of M_v at the i_{th} node and adjacent nodes required by Reynolds equation which form a finite difference operator can be calculated as in figure 5.3.

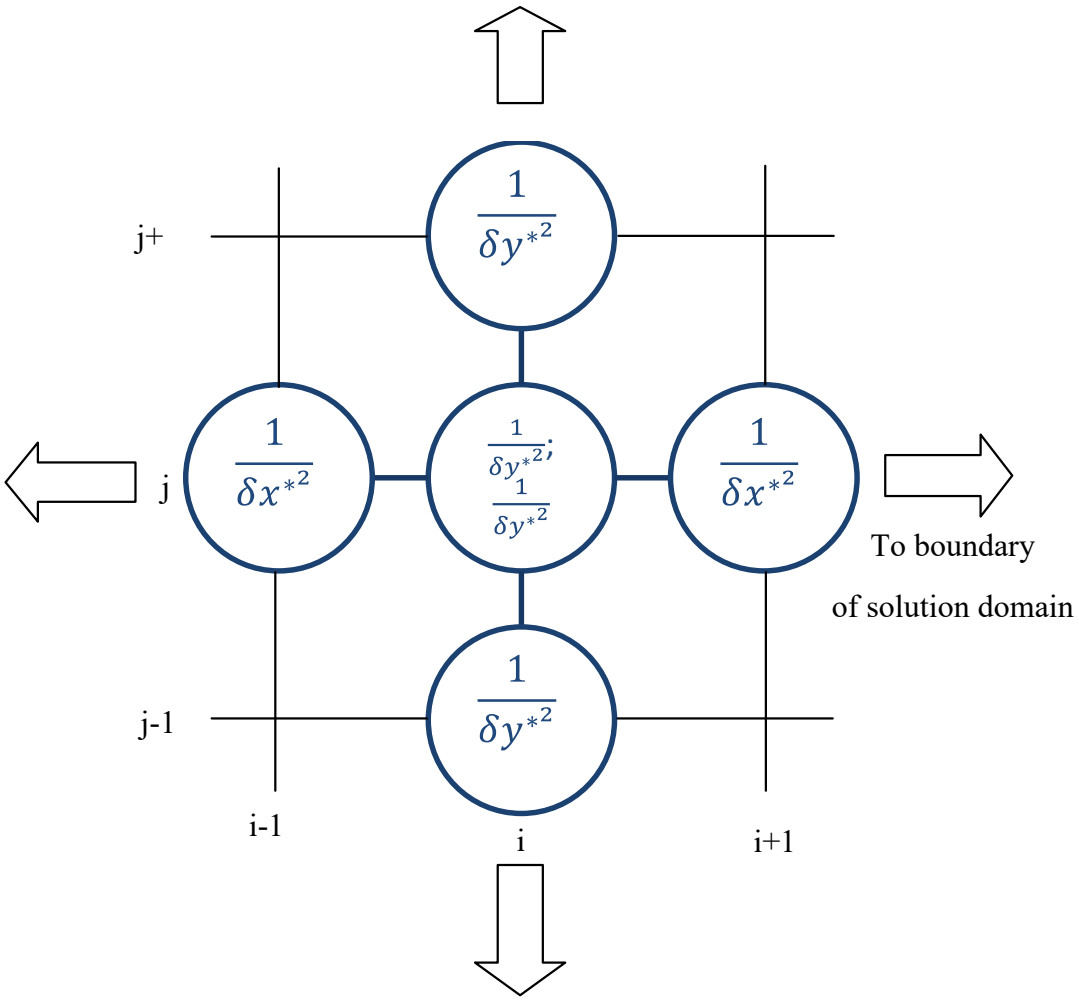

Figure 4.3 Finite difference operator and nodal scheme for numerical analysis of the Reynolds equation [46]

The finite difference operator is convenient for computation and it does not create difficulties with boundary conditions. A special arrangement of imaginary nodes outside the boundary is required for the finite difference operator located at the boundary. The solution domain is the range over which a solution is applicable, i.e. the dimensions of a bearing. The terms 'F' and 'G' are considered along with the finite difference operator to form a complete equivalent of the Reynolds equation. The equation thus obtained on rearrangement is given in equation 4.10.

$$M_{v,i,j} = \frac{C_1\left(M_{v,i+1,j}+M_{v,i-1,j}\right)+\left(\frac{R}{L}\right)^2 C_2\left(M_{v,i,j+1}+M_{v,i,j-1}\right)-G_{i,j}}{2C_1+2C_2+F_{i,j}} \qquad (4.10)$$

where $C_1 = \frac{1}{\delta x^{*2}}$

and $C_2 = \frac{1}{\delta y^{*2}}$

This expression is the basis for the finite difference solution for the Reynolds equation. Its solution gives the required nodal value of 'M_v'.

Definition of Solution Domain and Boundary Conditions

The next step after the establishment of controlling equations is the definition of boundary conditions and range of values to be computed. 'p^*' or 'M_v' is zero at the edges of a journal bearing and also cavitation prevents the occurrence of negative pressures in the bearing. For a complete bearing 'x^*' varies from 0 to 2π while for a partial the upper limit is smaller than 2π. 'y^*' varies from -0.5 to 0.5 as mid plane of bearing is selected as datum.

All the interior nodes require solution by finite difference method while the nodes on the edges of bearing have a pre-determined zero value. An extra column of nodes outside the solution domain is required for zero value consideration, when the solution is to be made over the half domain only as the nodes on the mid-line of the bearing are also variable. This extra column is generated by adopting node values from the column one step from the mid-line on the opposite side. In analytical terms this is achieved by setting:

$$M_{v_{i,jnode+1}} = M_{v_{i,jnode-1}} \tag{4.11}$$

where jnode is the number of nodes in j or y^* direction.

Splitting of solution domain helps in reducing the number of nodes but when analyzing a non-symmetric or misaligned bearing a domain covering complete bearing is necessary. In this case the domain is complete bearing with the limits 'y^*' from -0.5 to +0.5 and the mid- line boundary condition vanishes.

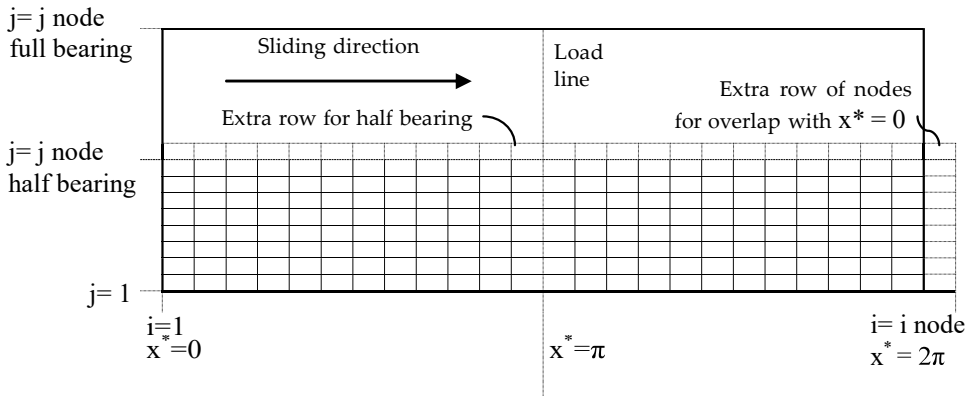

Figure 4.4 Nodal pressure domains for finite element analysis of hydrodynamic bearing

Calculation of Dimensionless Friction Force and Friction Coefficient

Friction force and friction coefficient are calculated from the film thickness and pressure gradient data. As discussed earlier in the previous chapter, the frictional force operating across the hydrodynamic film is calculated by integrating the shear stress 'τ' over the bearing area, i.e.:

$$F = \int_0^L \int_0^{2\pi R} \tau . dx . dy \tag{4.12}$$

where $$\tau = \frac{\eta U}{h} + \frac{h}{2}\frac{dp}{dx}$$

In the manner similar to hydrodynamic pressure, friction force has to be expressed in dimensionless form. On the substitution of dimensionless parameters into the equation, the expression for shear stress is given as in equation 4.13.

$$\tau = \frac{\eta U}{c}\left(\frac{1}{h^*} + 3h^*\frac{dp^*}{dx^*}\right) \tag{4.13}$$

where the last portion of the expression represents dimensionless form of shear stress τ^*.

So the expression for frictional force is obtained as in equation 4.14.

$$F = \frac{RL\eta U}{c}\int_0^1 \int_0^{2\pi} \tau^* dx^* dy^* = F^*\left(\frac{RL\eta U}{c}\right) \tag{4.14}$$

The coefficient of friction is the ratio of frictional force to the load acting on the bearing. Load on a journal bearing is given as in equation 4.15.

$$W = \int_0^L \int_0^{2\pi R} -\cos(x^*) . p . dx . dy \tag{4.15}$$

where the term –cos(x^*) rises from the fact the load supporting the pressure is located close to $x^*=\pi$ or $\cos(x^*)=1$. Any pressure close to $x^*=0$ merely imposes an extra load on the bearing as it acts in the direction of the load. The negative sign refers the fact that the load direction does not coincides with the direction of minimum film thickness.

The expression for load supported by the bearing is expressed in non-dimensional form in equation 4.16.

$$W = \frac{6U\eta R}{c^2} RL \int_0^1 \int_0^{2\pi} -\cos(x^*) p^* dx^* dy^* = W^* \left(\frac{6R^2 L\eta U}{c^2}\right) \tag{4.16}$$

From equation 4.14 and 4.16, the coefficient of friction can be gives as in equation 4.17.

$$\mu = \frac{F}{W} = \frac{c}{6R} \frac{F^*}{W^*} \tag{4.17}$$

The presence of cavitation in the bearing adds complication to the calculation of coefficient of friction. Within the cavitated region, the proportion of clearance space between shaft and bush that is filled by lubricant is represented by h^*_{cav}/ h^* where h^*_{cav} is the dimensionless film thickness at cavitation front and h^* is the dimensionless film thickness at specified position downstream of cavitation front.

Within the cavitated region 'p^*' and 'dp^*/dx^*' are equal to zero and the effective coefficient of friction is dependent on the fraction of lubricant filled in the clearance space. Under the assumption of simple proportionality between fluid filled volume and total shear force, the effective dimensionless shear stress τ_e^* that allows for zero shear stress between streamers of lubricant, is given by

$$\tau_e^* = \frac{h^*_{cav}}{h^{*2}} \tag{4.18}$$

The expression of non-dimensionless film thickness is given as in equation 4.19.

$$h^* = y^*.tcos(x^*) + \varepsilon \cos(x^* - \beta) + 1 \tag{4.19}$$

It is to be noted that the variation in 'h^*' due to misalignment is dependent on x^* whereas the variation in 'h^*' is also controlled by the attitude angle.

The derivatives of h^* are found by direct differentiation and are given as follows:

$$\frac{dh^*}{dx^*} = -y^* t sin(x^*) - \varepsilon \sin(x^* - \beta)$$

$$\frac{dh^*}{dy^*} = t cos(x^*)$$

$$\frac{d^2h^*}{dx^{*2}} = -y^* t cos(x^*) - \varepsilon \cos(x^* - \beta)$$

Numerical Solution Technique for Vogelpohl Equation

Gauss-Siedel iterative approach is utilized for the iterative solution. All the nodes are assigned an initial value of zero and finite difference equation (4.10) is repeatedly applied until the convergence is obtained.

4.4 Numerical analysis of hydrodynamic lubrication in idealized journal and partial arc bearings

The Reynolds equation (4.2) for the full and partial arc journal bearings were solved numerically to find the dimensionless pressure field corresponding to the equation 4.10 and other important bearing parameters. A computer program 'MISALIGNMENT' is generated for the calculations in software package MATLAB 2011. The flow chart of the computer program is depicted in figure 4.4. The program provides a solution for aligned as well as misaligned journal bearings. Misalignment has a pronounced effect on bearing characteristics but cannot be modeled by either the infinitely long or narrow bearing theories.

The program calculates the dimensionless load, attitude angle, and dimensionless (normalized) friction coefficient for a specified eccentricity, angle of partial arc bearing, 'L/D' ratio and misalignment ratio. The solution is based on an iso-viscous model of hydrodynamic lubrication with no elastic deflection of the bearing.

Program 'MISALIGNMENT' begins with a request for data input from the operator. The controlling variables are eccentricity 'ε', 'L/D' ratio, angle of partial arc and misalignment ratio. The values of relaxation factor, limiting residual, limiting number of iterations and node numbers in the 'i' and 'j' directions can be changed, as required, in the input data window.

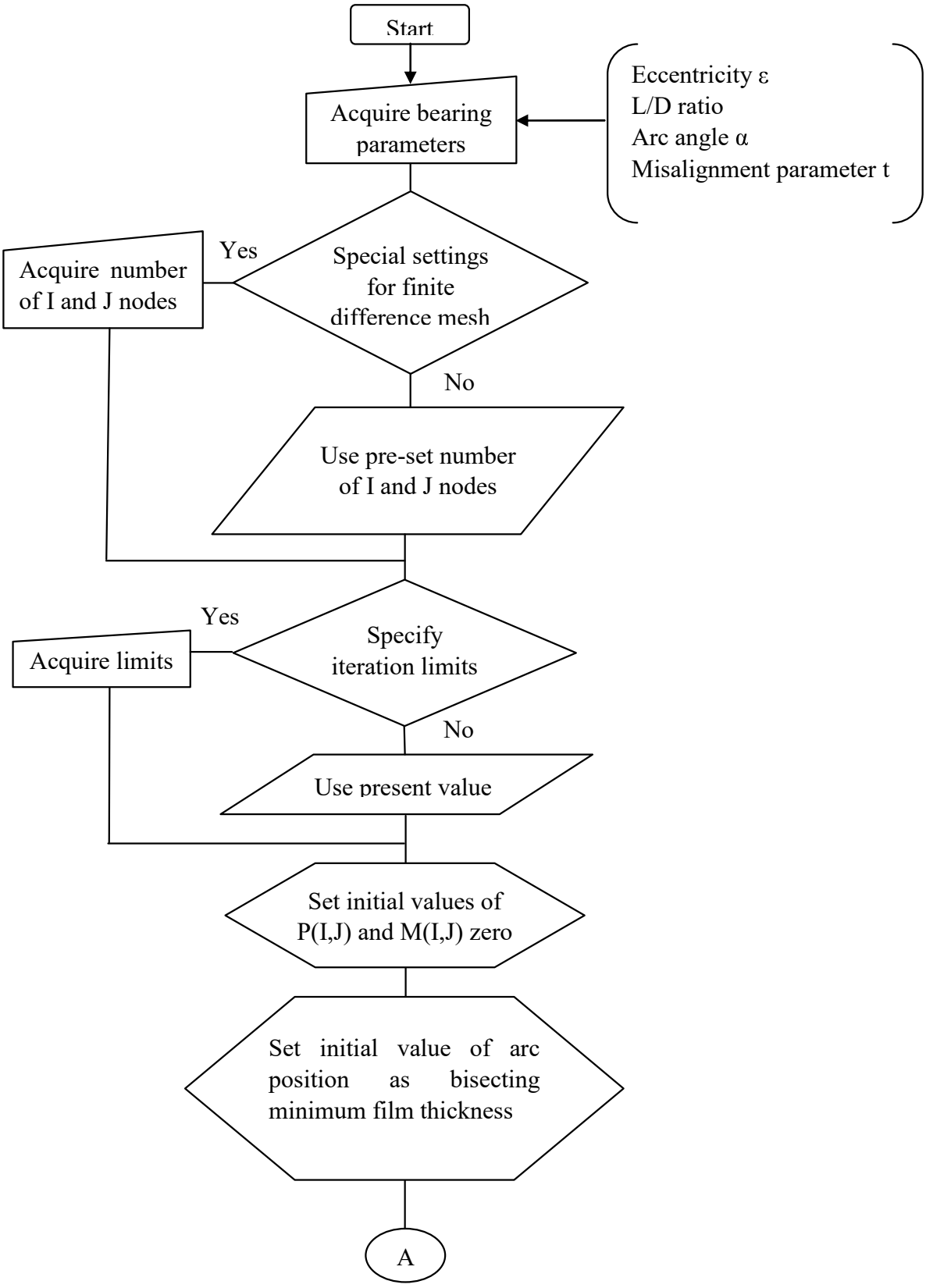
Start
Acquire bearing parameters
Eccentricity ε
L/D ratio
Arc angle α
Misalignment parameter t
Special settings for finite difference mesh
Yes
Acquire number of I and J nodes
No
Use pre-set number of I and J nodes
Specify iteration limits
Yes
Acquire limits
No
Use present value
Set initial values of P(I,J) and M(I,J) zero
Set initial value of arc position as bisecting minimum film thickness
A

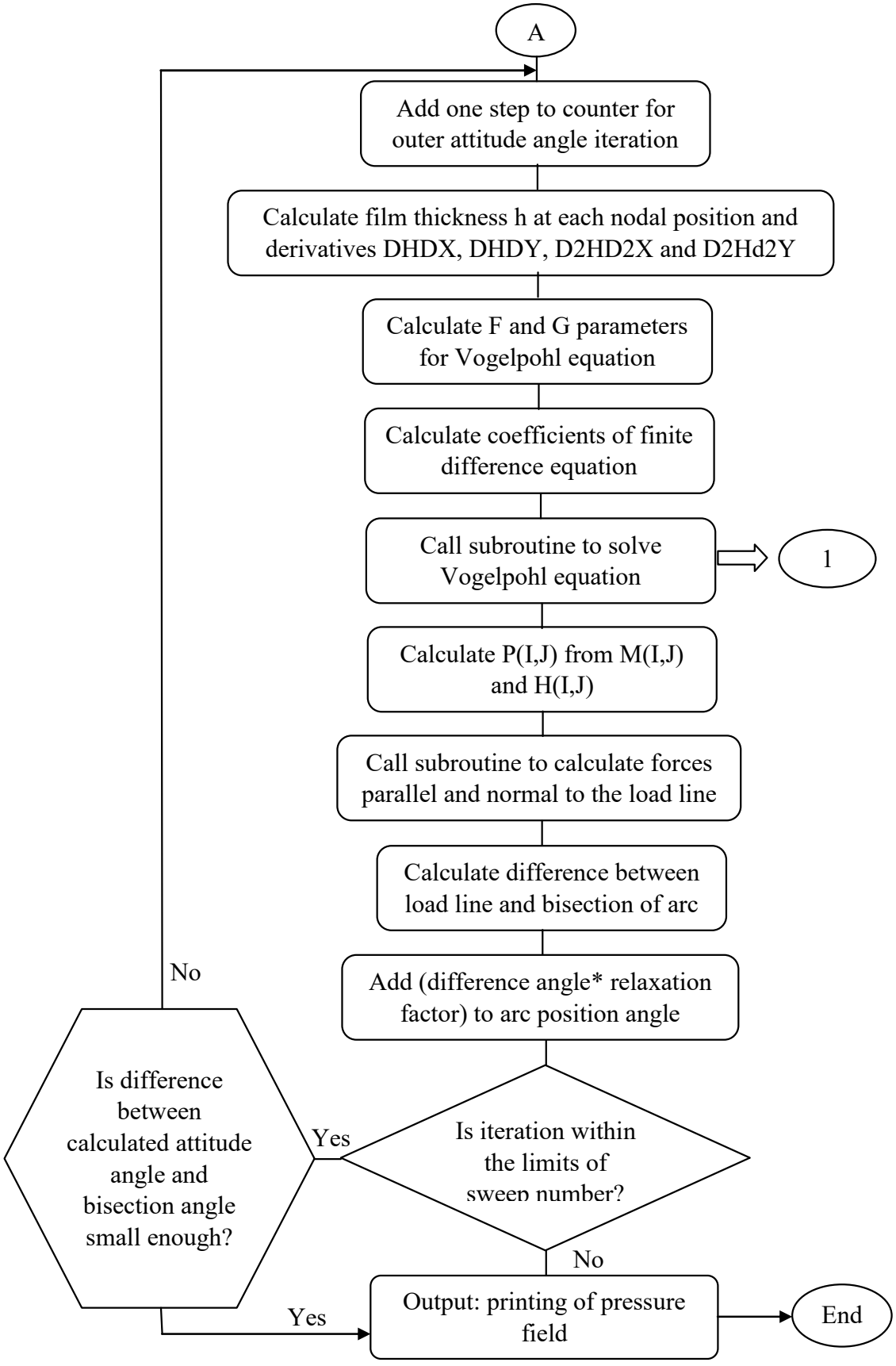
A
Add one step to counter for outer attitude angle iteration
Calculate film thickness h at each nodal position and derivatives DHDX, DHDY, D2HD2X and D2Hd2Y
Calculate F and G parameters for Vogelpohl equation
Calculate coefficients of finite difference equation
Call subroutine to solve Vogelpohl equation
1
Calculate P(I,J) from M(I,J) and H(I,J)
Call subroutine to calculate forces parallel and normal to the load line
Calculate difference between load line and bisection of arc
Add (difference angle* relaxation factor) to arc position angle
Is iteration within the limits of sweep number?
Yes
No
Is difference between calculated attitude angle and bisection angle small enough?
No
Yes
Output: printing of pressure field
End

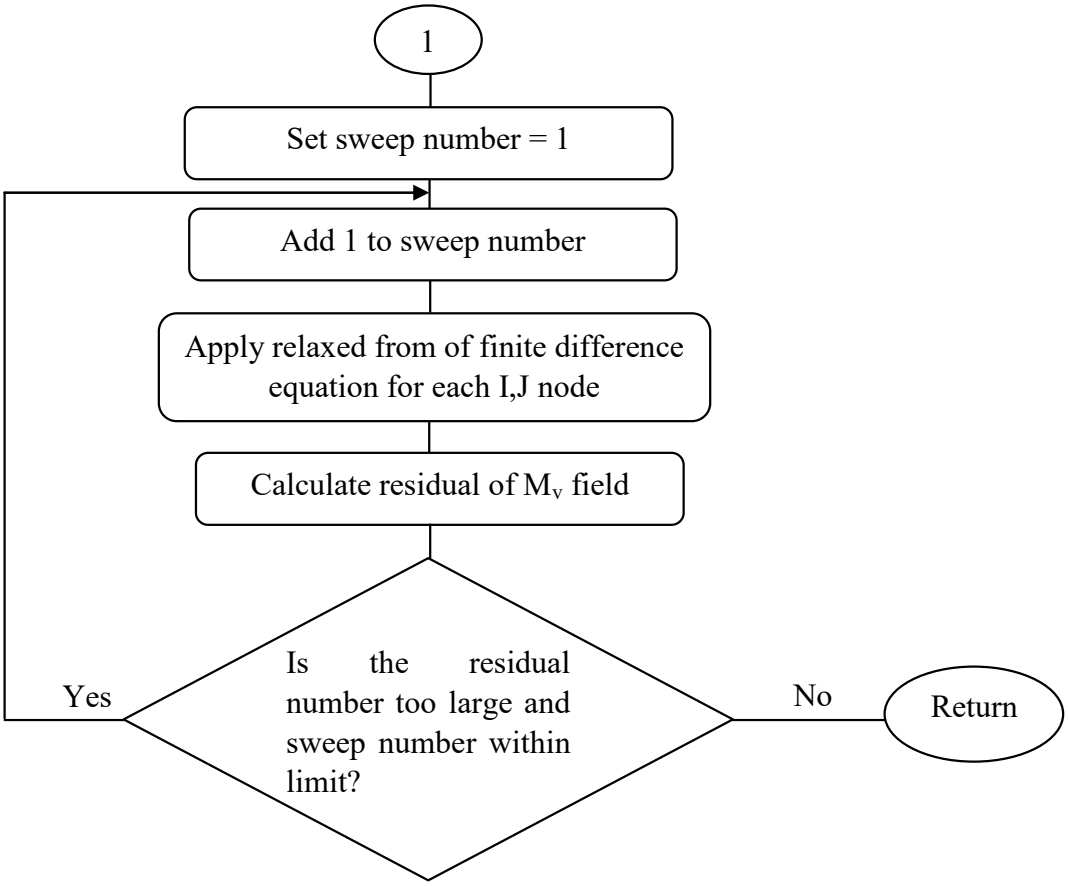

Figure 4.5 Program Flowchart for numerical analysis of hydrodynamic bearing using Matlab

Program Description

With all data recorded, the program proceeds to execution and in the first step a finite difference mesh is established. Values of 'δx^*' are generated by dividing the range of 'x^*' or 'y^*' by the number of steps between nodes, i.e.:

$$deltax = \frac{alpha}{inode - 1}; deltay = \frac{1}{jnode - 1}$$

where alpha is the angle subtended of partial arc bearing in radians

inode, jnode are the number of nodes in x and y direction respectively

deltax, deltay corresponds to δx^* and δy^*

The Vogelpohl parameter is assigned zero initial value at each node. Also, attitude angle 'beta' is assigned as zero. The solution of journal bearing requires two levels of iteration since the pressure or Vogelpohl parameter must be solved and the attitude angle is unknown. The attitude

angle ‘beta’ is thus iterated for as an outer level of iteration until the load calculated from the pressure field bisects the bearing.

The program enters the outer level of iteration for ‘beta’ as it reaches zero value. Now the values of ‘F(i,j)’ and ‘G(i,j)’ is calculated (equivalent of parameters ‘$F_{i,j}$’ and ‘$G_{i,j}$’). ‘dhdh0’ represents $\partial h^*/\partial x^*$, ‘dhdy0’ represents $\partial h^*/\partial y^*$, ‘d2hd2x0’ represents $\partial^2 h^*/\partial x^{*2}$ and ‘d2hd2y0’ represents $\partial^2 h^*/\partial x^{*2}$ whose values are calculated as per the expressions discussed in previous sections.

Next comes the iteration for ‘M(i,j)’. A parameter ‘sum’ is used to collect the total of values of ‘M(i,j)’ generated during one round of iteration. The parameter ‘sum’ is assigned an initial value of zero then a pair of nested ‘for’ loops commence the iteration for ‘M(i,j)’ within the range of ‘i’ from 2 to ‘inode-1’ and ‘j’ from 2 to ‘jnode-1’. This range of ‘i’ and ‘j’ covers all the nodes except those on the edge of the bearing.

The misaligned bearing is also analyzed in this program so that an entire bearing domain is covered by the iteration. The finite difference equation is modified to enable ‘over-relaxation’. Instead of ‘M(i,j)’, the value of the right-hand side of the equation 4.10 is assigned to a variable ‘store’. The final value of ‘M(i,j)’ is then calculated from:

$$M(i,j) = M(i,j) + factor1(store - M(i,j));$$

where the terms on the right hand side of the computing expression are the old values and the term on the left-hand side is the new value. The term ‘factor1’ is the Gauss-Seidel relaxation factor whose value is typically 1.3 for this iteration. The negative values of ‘M(i,j)’ generated are immediately suppressed by the statement:

$$\text{if } \mathrm{M(i,j)} < 0, \mathrm{M(i,j)} = 0; \text{ end;}$$

The final value of M(i,j) is then added to the term ‘sum’ from the statement:

$$sum = sum + M(i,j);$$

which completes the statements within the ‘for’ loop.

A residual is compiled outside of the ‘for’ loops, from the difference between the current value of ‘sum’ and a stored value ‘sum2’ from the previous round of iteration:

$$residp = abs((sum - sum2)/sum);$$

The value of ‘sum’ is then transferred to ‘sum2’ and ‘residp’ is tested to determine if it is below the convergence limit. To test convergence an inequality is used with a limit on the number of sweeps or iteration rounds included:

$$while\ (residp\ >\ reslim1)\ \&\ (n1\ <\ nlim1)$$

where reslim1 is the prescribed value of residual to terminate the iteration;

n1 is a counter variable for the number of sweeps;

nlim1 the limiting number of sweeps.

On the completion of iteration for Vogelpohl parameter, the program proceeds to the calculation for attitude angle. The pressure integral parallel and normal to the load-line are required for the calculation of attitude angle. The values of ‘P(i,j)’ are found from the following expression:

$$P(i,j)\ =\ M(i,j)/H(i,j)\text{^}1.5;$$

The calculations of the integrals are based on the ‘Trapezium rule’ with ‘P(i,j)’ multiplied by ‘-cos(x^*)’ for the pressure integral parallel to the load line and multiplied by ‘sin(x^*)’ for the film force pressure integral normal to the load line. The trapezium rule is applied by a ‘for’ statement where, at each node, the value of the function to be integrated at this node and the preceding node are added to the integral. ‘For’ statements runs from the second to the final node in any given line of nodal values to be integrated. In this way, all nodes except the first contribute twice the nodal value to the integral sum as required by the trapezium rule.

The film force term parallel to the load line is called ‘axialw’ and the normal film force is called ‘transw’. Integration is first performed in the ‘y^*’ direction to generate an array of integrals. The array is then multiplied by either ‘sin(x^*)’ or ‘cos(x^*)’ and integrated with respect to ‘x^*’.

The attitude angle can now be calculated from the arctangent of the ratio of ‘transw’ to ‘axialw’.

$$attang = atn(\frac{transw}{axialw});$$

where ‘attang’ is the attitude angle.

To allow the possibility of a negative axial film force where ‘attang1’ would be the negative, a conditional statement was also included of the above expression. The value of ‘beta’ was found

from over-relaxation of the attitude angle ‘attang1’ with the refinement that the desired value of ‘attang1’ has to be zero since the load vector should pass through 180°. This lead to the step:

$$beta = beta + factor2 * attang1;$$

A residual of the iteration in ‘beta’ was then calculated in a similar manner to the residual of the Vogelpohl parameter, i.e.:

$$residb = abs((beta - betas)/beta);$$

where ‘betas’ refers to the value of ‘beta’ from the previous iteration for ‘beta’. A conditional return to calculations of ‘F(i,j)’ and ‘G(i,j)’ was then based on whether ‘residb’ has reached the termination value and that the number of iteration rounds has not exceeded a predetermined limit.

The coefficient of friction was calculated in the final iteration. It begun with the search for a cavitation front defined by an array ‘ICAV(j)’. The values of ‘ICAV(j)’ were found by searching for zero ‘M(i,j)’ values in the down-stream direction and assigning to ‘ICAV(j)’ the first ‘i’ value where ‘M(i,j)’ is zero and ‘ICAV(j)’ still had a default value.

An array of dimensionless shear stress, ‘TORR(i,j)’, was then calculated with two expressions supplied for the cavitated and uncavitated regions of the bearing, i.e.:

$$if\ i < ICAV(j), TORR(i,j) = 1/H(i,j) + 3 * dpdx * H(i,j);\ end;$$

$$if\ i > ICAV(j), TORR(i,j) = H(i10,j)/H(i,j)\text{^}2;\ end;$$

where: dpdx refers to the local value of ‘dp*/dx*’ calculated by linear interpolation

i10 refers to the substitute for ‘ICAV(j)’ to simplify the array expression in the second statement

The values of dimensionless shear stress were then integrated by the same method which was used for the calculation of dimensionless load i.e. the trapezium form of numerical integration over ‘x^*’ and ‘y^*’. The friction force was obtained from the double integral over ‘x^*’ and ‘y^*’. The dimensionless friction coefficient was then calculated.

Upon the completion of iterations for both the vogelpohl parameter and attitude angle, and the coefficient of friction determined, the final task is to depict the values of load and pressure profile for the bearing. All pressures were depicted as the percentage of maximum pressure to avoid any difficulties in format for large range of dimensionless pressure.

4.5 Vibrational stability in journal bearing

As discussed in the previous chapter, hydrodynamic bearings are prone to a vibrational instability termed as 'oil whirl'. A series of stiffness and damping coefficients are used to model the vibrational characteristics of a hydrodynamic film. These coefficients can be computed from the solutions of the Reynolds equation.

A simpler mode of analysis for practical engineering applications is used. Routh-Hurwitz criterion of stability is used to calculate limiting shaft speed at the onset of vibrations. The criterion provides a conservative estimate of the shaft speed at which some level of sustained vibration occurs. It has often been found that at moderate shaft speeds, shaft vibration may occur but it is limited to finite and safe amplitudes. On the other hand at higher speeds, there is no limit to the amplitude of vibration and the shaft will oscillate in ever wider trajectories until it touches the bush which inevitably results in destruction of the bearing.

In order to analyze shaft trajectories, the non-linear variation in stiffness and damping coefficients with shaft position must be included in the analysis. The advantage of the Routh-Hurwitz method is that only infinitesimal amplitudes of vibration are considered which allow the use of linearized stiffness and damping coefficients. The linearized Routh-Hurwitz analysis of bearing vibration and the computation method is described in the following sections.

4.5.1 Determination of Stiffness and Damping Coefficients

Stiffness and damping coefficients are obtained by including in the Reynolds equation the effect of small displacements and squeeze velocities. Stiffness and damping coefficients are calculated from the change in pressure integral, by dividing the changes by the displacement and squeeze velocity respectively. Magnitudes of displacements and squeeze velocities are held at small values in order to minimize inaccuracy due to non-linear variation of film forces. A cartesian coordinate system aligned with the direction of bearing load, shown in Figure 4.6, is established and values of stiffness and damping coefficients normal and co-directional with the load-line are

then computed. Four stiffness coefficients relating to the range of possible bearing movements 'K_{xx}', 'K_{yy}', 'K_{xy}' and 'K_{yx}' and four damping coefficients 'C_{xx}', 'C_{yy}', 'C_{xy}' and 'C_{yx}' are required for vibration analysis. To find these coefficients the effect of small displacements on hydrodynamic pressure integral must be analyzed.

Shaft displacements are modelled in the Reynolds equation in terms of their effect on dh/dx. It is convenient to use non-dimensional forms of shaft displacement in terms of the radial bearing clearance, i.e.:

$$\Delta x^* = \frac{\Delta x}{c} \tag{4.20}$$

Where Δx refers to the displacement of shaft center in x direction

c refers to the radial clearance of the bearing

Δx^* refers to the non-dimensional displacement

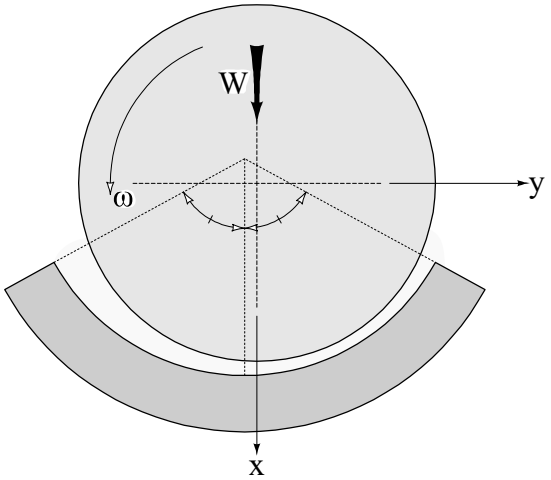

Figure 4.6 Journal bearing coordinate configuration for vibration analysis

A similar relationship applies to 'Δy', the displacement in the 'y' direction. The equation for dh^*/dx^* is given in the following form according to basic geometrical principles:

$$\frac{\partial h^*}{\partial x^*} = \left(\frac{\partial h^*}{\partial x^*}\right)_{static} + \frac{\partial(\Delta x^* cos(x^*) + \Delta y^* \sin(x^*))}{\partial x^*} \tag{4.21}$$

where x^* refers to the film ordinate around bearing

$\left(\frac{\partial h^*}{\partial x^*}\right)_{static}$ refers to the variation in film thickness for static case

The modified forms of 'h^*' and '$\partial^2 h^*/\partial x^{*2}$' which are required for the Vogelpohl equation follow the scheme already described and are given in equation (4.22) and (4.23)

$$h^* = h^*_{static} + \Delta x^* cos(x^*) + \Delta y^* sin(x^*) \tag{4.22}$$

$$\frac{\partial^2 h^*}{\partial x^{*2}} = \left(\frac{\partial^2 h^*}{\partial x^{*2}}\right)_{static} + \frac{\partial^2}{\partial x^2}(\Delta x^* cosx^* + \Delta y^* sinx^*) \tag{4.23}$$

The Vogelpohl equation (4.4) is then solved in terms of the modified forms of 'h^*' and its derivatives, i.e. $\partial h^*/\partial x^*$, $\partial h^*/\partial y^*$ etc. Non-dimensional stiffness coefficients are defined as follows:

$$K^* = \frac{K_c}{W} \tag{4.24}$$

where K* refers to the non-dimensional stiffness

K refers to the real stiffness

c refers to the radial clearance of the bearing

W refers to the bearing load

This form of non-dimensionalization can be shown to be equivalent to:

$$K^* = \frac{\Delta W^*}{\Delta x^* W^*_{static}} \tag{4.25}$$

Since '$\delta \mathbf{x}^*$' is very small then:

$$W^* \approx W^*_{static} \tag{4.26}$$

In other words, non-dimensional stiffness coefficients are equal to the change in non-dimensional load divided by the product of non-dimensional displacement and static non-dimensional load. The change in load 'ΔW^*', is calculated from the total load found by integration of the hydrodynamic pressure field with the displacement parameters included, and the static load, i.e.:

$$\Delta W^* = W^* - W^*_{static} \tag{4.27}$$

In exact terms, only the change in film force along the '**x**' or '**y**' axis is calculated not the change in the total load. For example, 'K_{xx}^*' stiffness is calculated according to the following equation, i.e.:

$$K_{xx}^* = \frac{\Delta W_x^*}{\Delta x^* W^*} \tag{4.28}$$

where 'ΔW_x^*' refers to the load change in the 'x' direction

Similarly, K_{yx}^* is given as in equation (4.29)

$$K_{yx}^* = \frac{\Delta W_y^*}{\Delta x^* W^*} \tag{4.29}$$

where 'ΔW_y^*' refers to the load change in the 'y' direction

Similarly, other stiffness coefficients can be calculated.

Damping coefficients are found by adding appropriate squeeze terms to the Reynolds equation. A non-dimensional squeeze term is defined as:

$$w^* = \frac{w}{c\omega} \tag{4.30}$$

where w refers to the squeeze velocity in

c refers to the radial clearance

ω refers to the angular velocity of the shaft

The non-dimensional form of Reynolds equation with squeeze terms is given as follows:

$$\frac{\partial}{\partial x^*}\left(h^{*3}\frac{\partial p^*}{\partial x^*}\right) + \left(\frac{R}{L}\right)^2 \frac{\partial}{\partial y^*}\left(h^{*3}\frac{\partial p^*}{\partial y^*}\right) = \frac{\partial h^*}{\partial x^*} + 2w^* \tag{4.31}$$

The squeeze velocity is not constant around the hydrodynamic film but varies in a sinusoidal manner similar to the displacements. An expression for the dimensionless squeeze velocity at any position on the hydrodynamic film in terms of squeeze velocities along the 'x' and 'y' axes is given by:

$$w^* = w_x^* cosx^* + w_y^* sinx^* \tag{4.32}$$

The squeeze term 'w^*' can be included in the parameter 'G' of the Vogelpohl equation, i.e.:

$$\frac{\partial^2 M_v}{\partial x^{*2}} + \left(\frac{R}{L}\right)^2 \frac{\partial^2 M_v}{\partial y^{*2}} = FM_v + G = \frac{FM_v + \frac{\partial h^*}{\partial x^*} + 2w^*}{h^{*1.5}} \tag{4.33}$$

Damping coefficients are computed in a similar manner to the stiffness coefficients, i.e. an arbitrary infinitesimal squeeze velocity is applied to cause a change in the pressure integral. The non-dimensional damping coefficient is defined in a similar manner to the non-dimensional stiffness coefficient, i.e.:

$$C^* = C\left(\frac{c\omega}{W}\right) \tag{4.34}$$

where C^* refers to the non-dimensional damping coefficient

C refers to the real damping coefficient

In terms of non-dimensional quantities, the non-dimensional damping coefficient can be expressed as in equation (4.35).

$$C^* = \left(\frac{\Delta W^*}{w^* W^*}\right) \tag{4.35}$$

The specific damping coefficient can be calculated as in equation (4.36).

$$C^*_{xx} = \left(\frac{\Delta W^*_x}{w^*_x W^*}\right) \tag{4.36}$$

After determining all the necessary values of stiffness and damping coefficients the vibrational stability of a bearing can be evaluated. There are various theories of bearing vibrational analysis and the obtained stiffness and damping coefficients can be used in any of these methods. The method developed by Hori [47] has been used in this analysis. In this theory a simple disc of a mass ‘m’ mounted centrally on a shaft supported by two journal bearings is considered. The disc tends to vibrate in the ‘x’ and ‘y’ directions which are both normal to the shaft axis. The configuration is shown in Figure 4.7.

There are two sources of disc deflection in this model; the shaft can bend and the two bearings are of finite stiffness which allows translation of the shaft. This system was analyzed by Newton's second law of motion to provide a series of equations relating the acceleration of the rotor in either the ‘x’ or the ‘y’ direction to the mass of the disc, shaft and bearing stiffnesses, and bearing damping coefficients. The description of this analysis can be found in [ ].

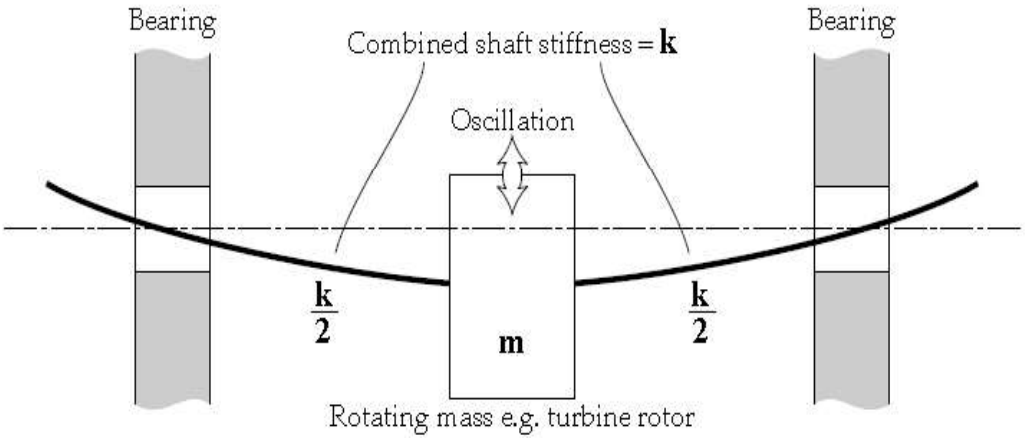

Figure 4.7 Hori's model for journal bearing analysis [47]

The equations of motion of the disc can be solved to produce shaft trajectory but this is not often required since the most important information resulting from the analysis is the limiting shaft speed at the onset of bearing vibration. The limiting shaft speed is derived from the Routh-Hurwitz criterion which provides the following expression for the 'threshold speed of self-excited vibration' or the 'critical frequency' as it is often called:

$$\omega_c^{*2} = \frac{A_1 A_3 {A_5}^2}{({A_1}^2 + A_2 {A_5}^2 - A_1 A_4 A_5)(A_5 + \gamma A_1)} \tag{4.37}$$

where A_1, A_2, A_3, A_4, A_5 refers to the dimensionless stiffness and damping products

ω_c^* refers to the dimensionless bearing critical frequency

The bearing critical frequency is also given by:

$$\omega_c^* = \frac{\omega_c}{(\frac{g}{c})^{0.5}} \tag{4.38}$$

where ω_c refers to the angular speed of the shaft

g refers to the acceleration due to gravity

c refers to the radial clearance of the bearing

and the γ parameter can be expressed as in equation 4.39.

$$\gamma = \frac{W}{kc} \tag{4.39}$$

where W refers to the weight on the shaft

k refers to the stiffness of the shaft

Since the 'γ' parameter is independent of bearing geometry is must be specified before commencing computing of a solution to equation (4.37).

The 'A' terms relate to stiffness and damping coefficients in the following manner [ ]:

$$A_1 = K^*_{xx}C^*_{yy} - K^*_{xy}C^*_{yx} - K^*_{yx}C^*_{xy} + K^*_{yy}C^*_{xx}$$

$$A_2 = K^*_{xx}K^*_{yy} - K^*_{xy}K^*_{yx}$$

$$A_3 = C^*_{xx}C^*_{yy} - C^*_{xy}C^*_{yx}$$

$$A_4 = K^*_{xx} + K^*_{yy}$$

$$A_5 = C^*_{xx} + C^*_{yy}$$

The analysis is completed with the calculation of the non-dimensional critical frequency 'ω_c'.

4.5.2 Computer Program for the Analysis of Vibrational Stability in a Partial Arc Journal Bearing

A computer program 'STABILITY' for analysis of vibrational stability in a partial arc journal bearing is listed and described in the Appendix and its flow chart is shown in Figure 4.8. The program computes the limits of bearing vibrational stability. The Vogelpohl equation is solved by the same method described for the program 'MISALIGNMENT'.

Program Description

Program 'STABILITY' begins with the standard input requests for values of the eccentricity ratio, 'L/D' ratio, angle of partial arc and misalignment ratio. The dimensionless exciter mass is also required in this program. The dimensionless exciter mass refers to the rotating mass of the shaft or attached disc which provides the energy for vibration.

The program then proceeds to solve the Vogelpohl equation according to the steps adapted from the program 'MISALIGNMENT' with a small modification. 'SWITCH1(i,j)' function is used inside the iteration subroutine to exempt cavitated nodes from the iteration.

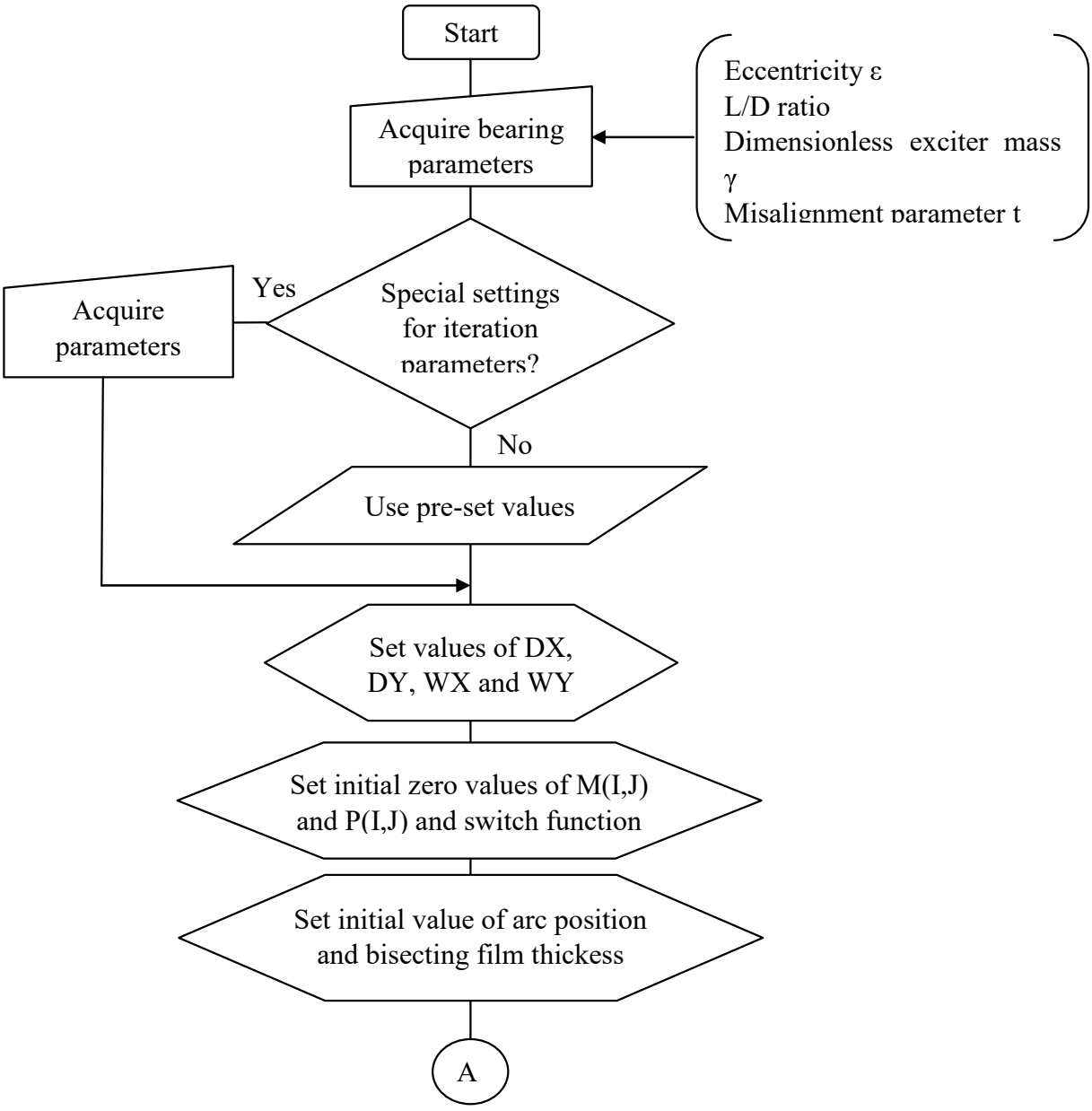
Start
Acquire bearing parameters
Eccentricity ε
L/D ratio
Dimensionless exciter mass γ
Misalignment parameter t
Special settings for iteration parameters?
Yes
Acquire parameters
No
Use pre-set values
Set values of DX, DY, WX and WY
Set initial zero values of M(I,J) and P(I,J) and switch function
Set initial value of arc position and bisecting film thickess
A

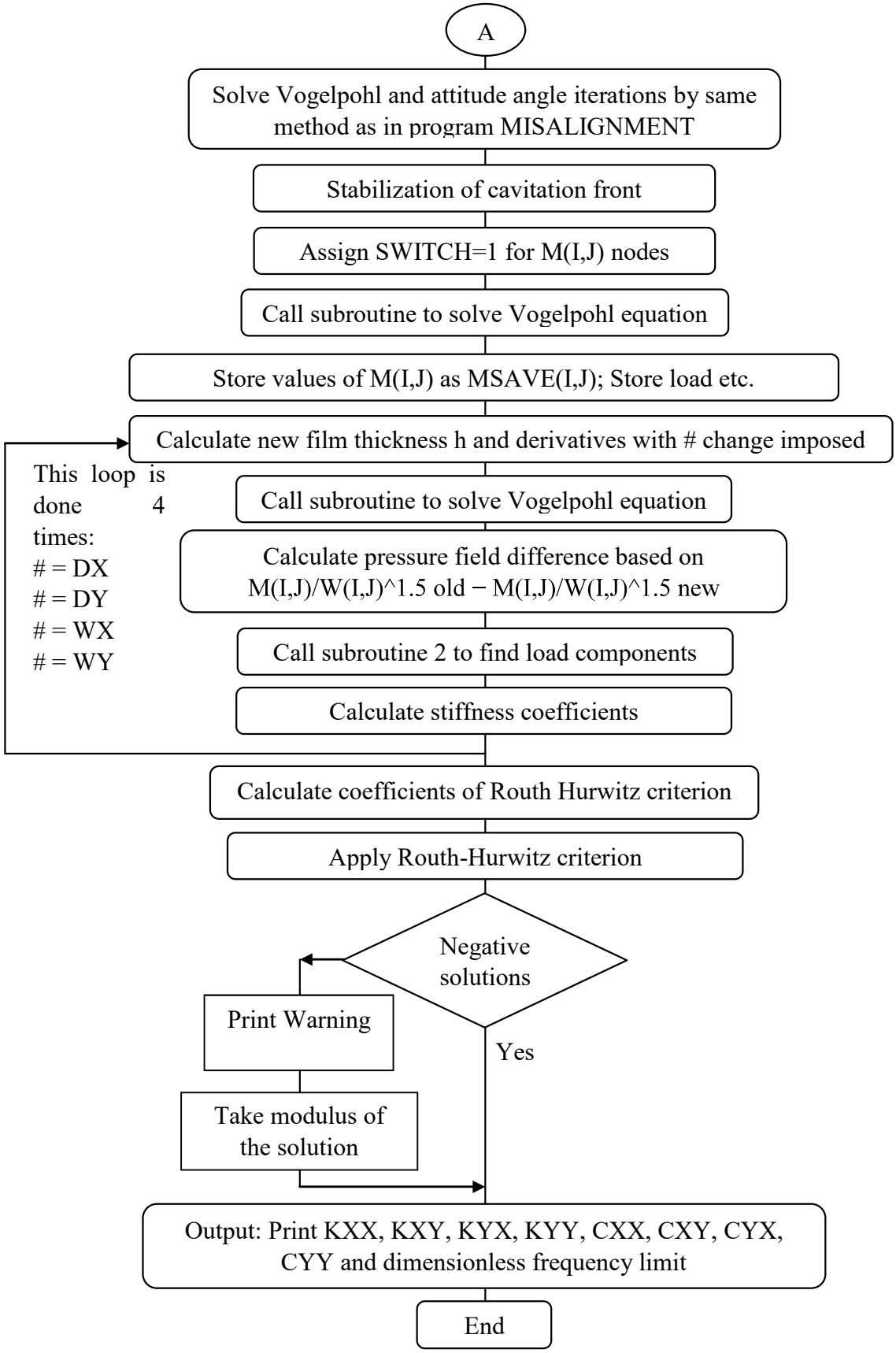

Figure 4.8 Flowchart for the stability analysis in a journal bearing

This variable is only activated, i.e. non-zero values assigned to further iteration, after completion of the iteration for the static case. The purpose of 'SWITCH1(i,j)' is to prevent any oscillation of the cavitated region during calculation of stiffness and damping coefficients. Calculation of these coefficients is based on very small differences between the equilibrium pressure field and a perturbed pressure field resulting from small displacements and squeeze velocities. Accurate values of the coefficients are only obtained when the static or equilibrium pressure field is iterated to a high degree of accuracy. To meet this requirement, once the initial double iteration for pressure field and attitude angle is completed, cavitated nodes are isolated.

Values of 'F' and 'G' in the Vogelpohl equation are then calculated with the final value of 'β' from the attitude angle iteration. The iteration for 'M(i,j)' is then repeated once more to eliminate any possible errors caused by a mobile cavitation front. When these steps are completed, it is found that accurate values of 'M(i,j)' are obtained. The final values of 'M(i,j)' are then stored in an array 'MSAVE(i,j)'. The program then proceeds to the calculation of stiffness and damping coefficients via the introduction of infinitesimal displacements, 'dx' and 'dy', and squeeze velocities, 'w0x' and 'w0y'. The solution for 'M(i,j)' with perturbations begins with calculations of 'F(i,j)' and 'G(i,j)' with the perturbations included. In general, the perturbations refer to displacements or squeeze velocities. The displacements 'dx', 'dy' and squeeze velocities 'w0x' and 'w0y' are applied in order to find the stiffness 'kxx', 'kyx', 'kyy', 'kxy' and damping 'cxx', 'cyx', 'cyy', 'cxy' coefficients. For a given perturbation, once the values of 'F(i,j)' and 'G(i,j)' have been calculated then the subroutine for the iteration of 'M(i,j)' is applied.

The array 'P(i,j)' is used to store the difference in pressures rather than the absolute value of pressures so that it can be read directly in the subroutine for load integration to find the stiffness or damping coefficients. The value of 'H(i,j)' of the perturbed solution must also include the displacement which in the example shown above is 'dy'. If this were omitted inaccurate values of stiffness would be obtained. For squeeze perturbations, the film thickness is identical to the static case. The difference in load capacity is then obtained by applying the load integration subroutine to the values of 'P(i,j)'. The values of stiffness coefficients, e.g. 'kxx' and 'kxy' are then found by applying the following steps:

$$kxx = axialw/(dx * loadw);\ kyx = -transw/(dx * loadw);$$

An analogous set of statements is employed to calculate the damping coefficients. For example, the damping coefficients 'Cxx*' and 'Cyx*' are calculated according to the following steps:

$$cxx = axialw/(w0x * loadw1);\ cyx = -transw/(w0x * loadw1);$$

Once the values of stiffness and damping coefficients are known, the program then proceeds to calculate the dimensionless critical frequency by applying equations (4.37-4.39). The program concludes with a print-out of the values of dimensionless critical frequency, stiffness and damping coefficients.

Chapter 5

Results and Discussions

Computer programs have been developed for the software package Matlab to predict the effect of misalignment in a journal bearing. Numerical simulations have been carried out to analyse the effect of misalignment on the bearing parameters like load carrying capacity, maximum pressure, film thickness and attitude angle using the program 'MISALIGNMENT'. Also the influence of misalignment on the vibrational stability of bearing is analysed using the program 'STABILITY'. Numerical simulations have been carried out to analyse the effect of misalignment on stiffness and damping parameters using this program.

The main specifications of the bearing model and lubricant used in the calculation are given in Table 5.1. This model had been used by Bouyer et. al. to experimentally find out the effect of misalignment in a hydrodynamic plane journal bearing[24].

S.No.	Parameter	Value
1.	Bearing diameter	0.099780m
2.	Bearing length	0.080m
3.	Radial clearance	0.0001175m
4.	L/D	0.8
5.	Speed	4000 rpm
6.	Oil supply Temperature	40°C
7.	Lubricant grade	ISO VG 32
8.	Density	870 kg/m^3
9.	Specific heat	2000 J/kgK
10.	Viscosity (@40°C)	0.0293 Pa-s

Table 5.1 Input parameters

The characteristics of the bearing were calculated for a full journal bearing with different eccentricity ratios considering and without considering the misalignment effect. Misalignment parameter was varied from 0 to 0.2 for the analysis of misaligned journal bearing. The results obtained have been discussed further.

The iterations were carried out with 100 nodes in both x and y directions. The terminating value for residual for iterations to solve Vogelpohl equation and attitude angle were set to 0.000001 and 0.0001 respectively. The relaxation factors for both the iterations were set to 1.2 and 1 respectively. The maximum number cycles for both the iterations are limited to 100.

S.No.	Eccentricity Ratio	Dimensionless load for misalignment parameter t=0	Dimensionless load for misalignment parameter t=0.1	Dimensionless load for misalignment parameter t=0.2
1.	0.1	0.028154	0.028238	0.028284
2.	0.3	0.096704	0.095815	0.096068
3.	0.5	0.21585	0.2162	0.21272
4.	0.7	0.53318	0.53588	0.54425
5.	0.9	2.4729	2.6496	4.0948

Table 5.2 Variation in dimensionless load for different eccentricity ratios

S.No.	Eccentricity Ratio	Dimensionless maximum pressure for misalignment parameter t=0	Dimensionless maximum pressure for misalignment parameter t=0.1	Dimensionless maximum pressure for misalignment parameter t=0.2
1.	0.1	0.026253	0.026357	0.026504
2.	0.3	0.097539	0.096671	0.097149
3.	0.5	0.24924	0.25024	0.25863
4.	0.7	0.75334	0.76524	0.80365
5.	0.9	5.2888	7.0263	51.853

Table 5.3 Variation in dimensionless maximum pressure for different eccentricity ratios

Now using equation for the dimensionless load, the load on the bearing was calculated according to the equation (4.16).

$$W = W^*(\frac{6R^2L\eta U}{c^2})$$

Similarly the maximum pressure was calculated using equation

$$p = p^*(\frac{6R\eta U}{c^2})$$

The variation in the maximum pressure due to misalignment is depicted using the following graph.

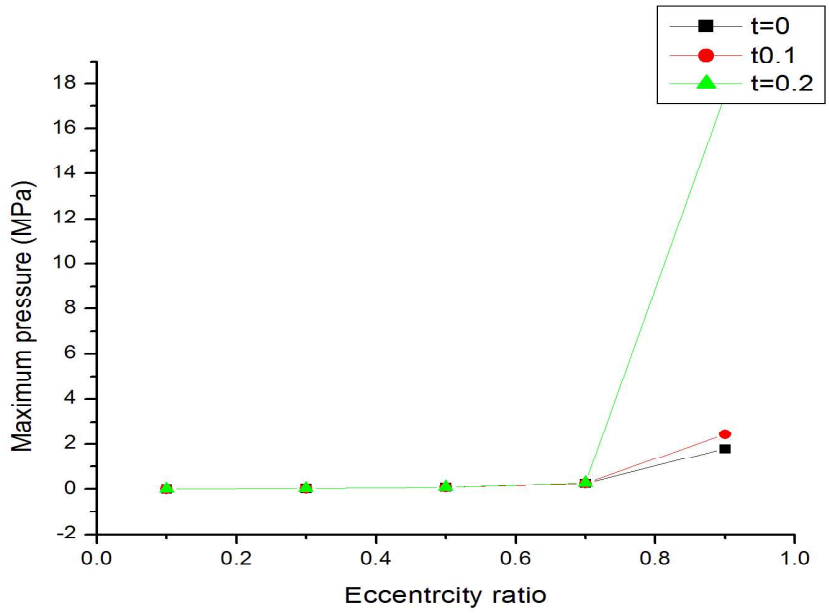

Figure 5.1 Graph for the variation in maximum pressure with eccentricity ratio

From the graph, it can be concluded that the maximum pressure in fluid film bearing is affected by the misalignment of shaft. Misalignment has much more severe effects at high values of eccentricity ratio.

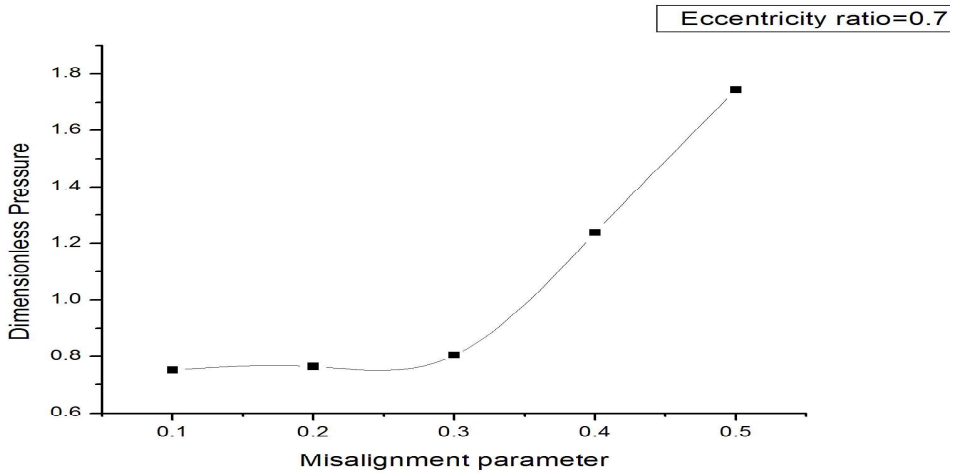

Figure 5.2 Graph for variation in pressure with misalignment parameter

S.No.	Eccentricity Ratio	Dimensionless friction coefficient for misalignment parameter t=0	Dimensionless friction coefficient for misalignment parameter t=0.1	Dimensionless friction coefficient for misalignment parameter t=0.2
1.	0.1	230.62	230.13	230.68
2.	0.3	83.703	84.518	84.724
3.	0.5	58.105	58.196	59.863
4.	0.7	49.807	50.085	50.976
5.	0.9	9.4703	9.5959	4.3108

Table 5.4 Variation in dimensionless friction coefficient for different eccentricity ratios

Also the value of coefficient of friction was obtained using equation (4.17)

$$\mu = \frac{F}{W} = \frac{c}{6R}\frac{F^*}{W^*}$$

S.No.	Eccentricity Ratio	Attitude angle for misalignment parameter t=0	Attitude angle for misalignment parameter t=0.1	Attitude angle for misalignment parameter t=0.2
1.	0.1	83.306°	83.569°	83.509°
2.	0.3	70.396°	70.675°	70.687°
3.	0.5	57.256°	57.26°	56.842°
4.	0.7	43.238°	43.202°	43.098°
5.	0.9	25.555°	24.825°	19.973°

Table 5.5 Variation in attitude angle coefficient for different eccentricity ratios

From table 5.5, the variation in the attitude angle for different values of misalignment can be obtained. It has been found that the attitude angle decreases with increase in misalignment. However, the effect is more prominent for higher values of eccentricity ratio.

The pressure fields for the bearing for the different values of eccentricity ratio and misalignment parameter were obtained. The pressure distribution obtained for eccentricity ratio equal to 0.1 is shown in the figure below.

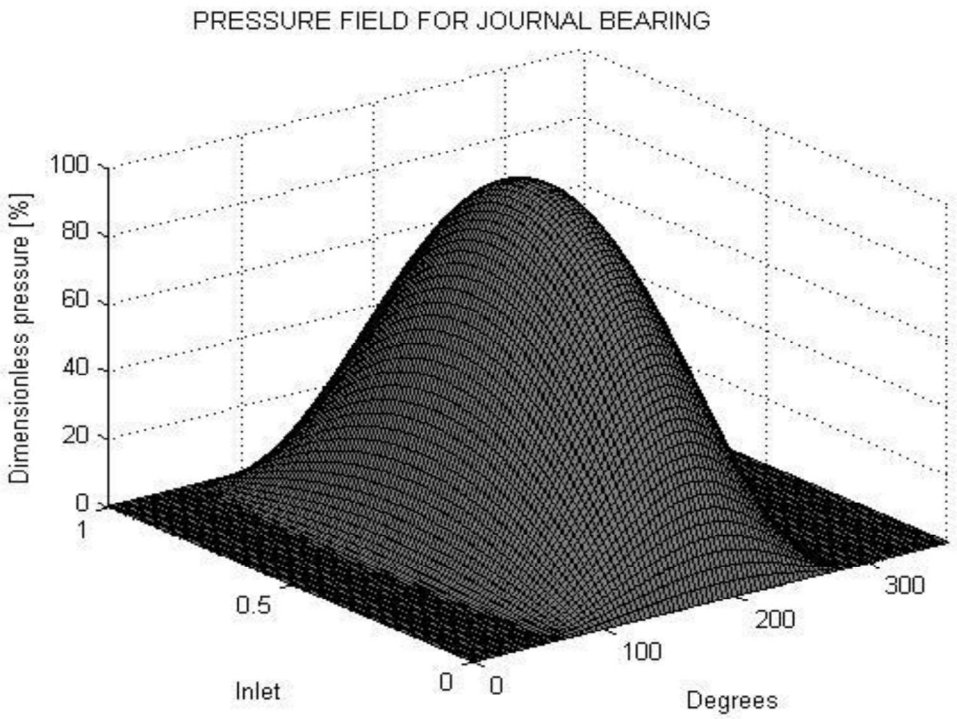

Figure 5.3 Pressure field for ε=0.1 and t=0

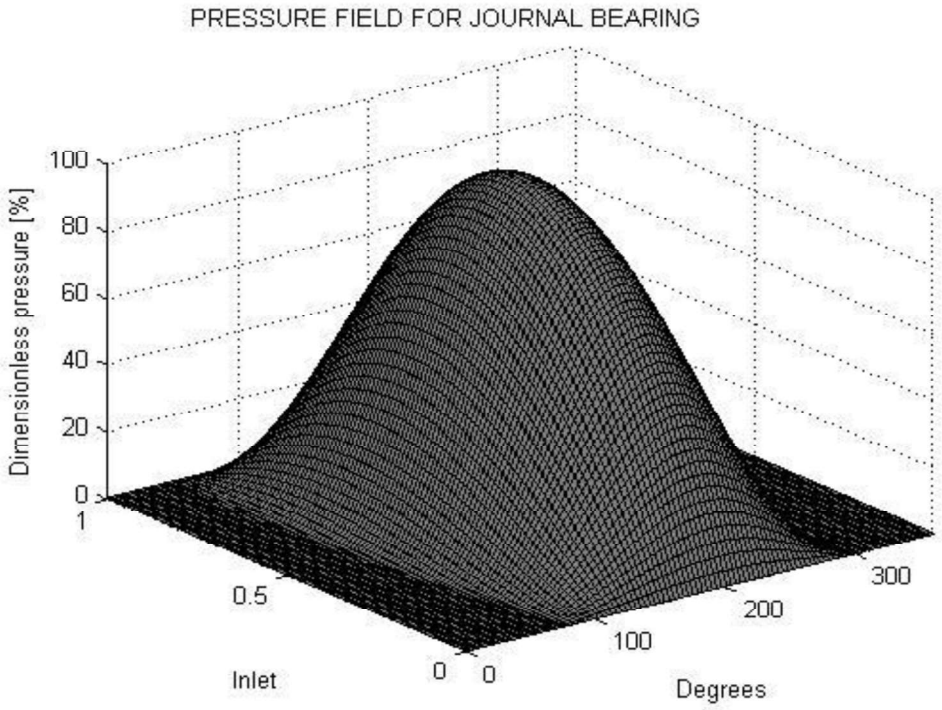

Figure 5.4 Pressure field for ε=0.1 and t=0.1

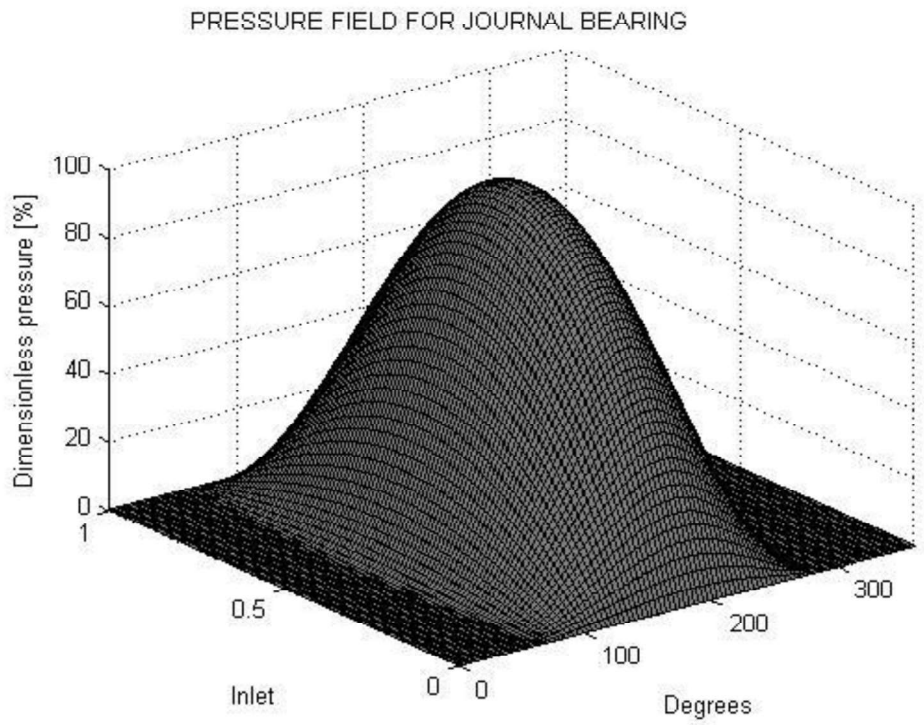

Figure 5.5 Pressure field for ε=0.1 and t=0.2

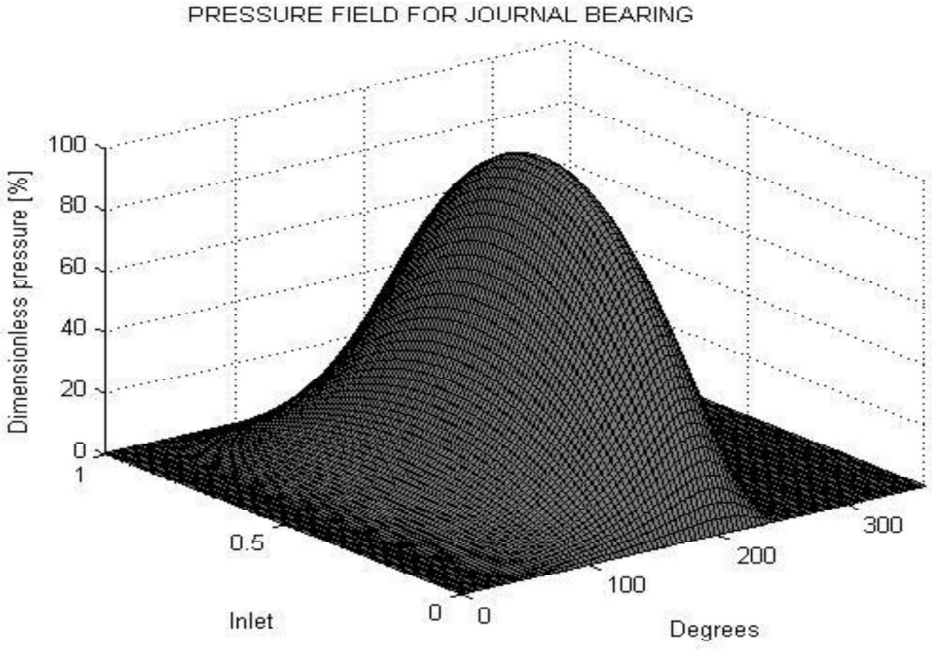

Figure 5.6 Pressure field for ε=0.5 and t=0

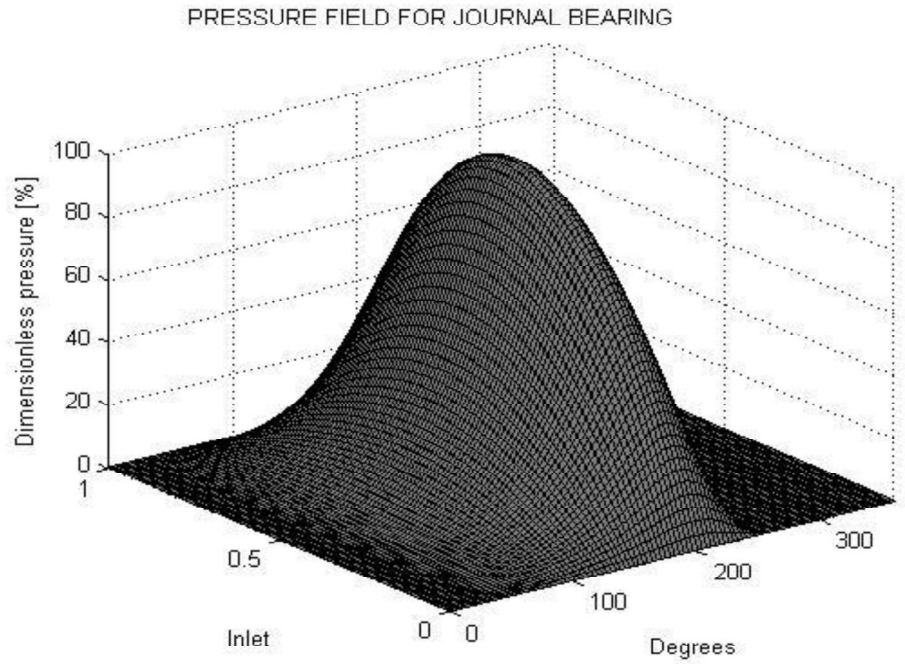

Figure 5.7 Pressure field for ε=0.5 and t=0.1

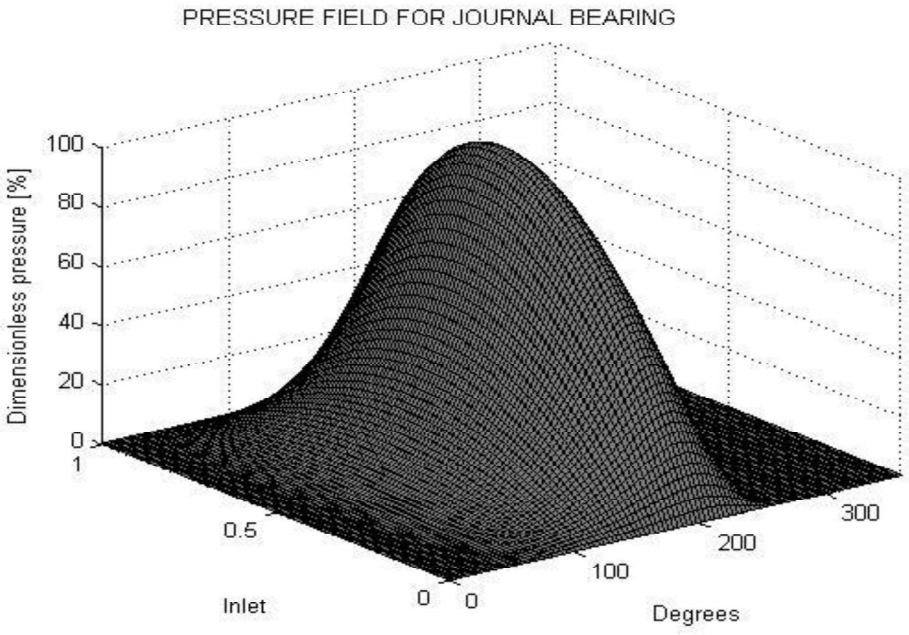

Figure 5.8 Pressure field for ε=0.5 and t=0.2

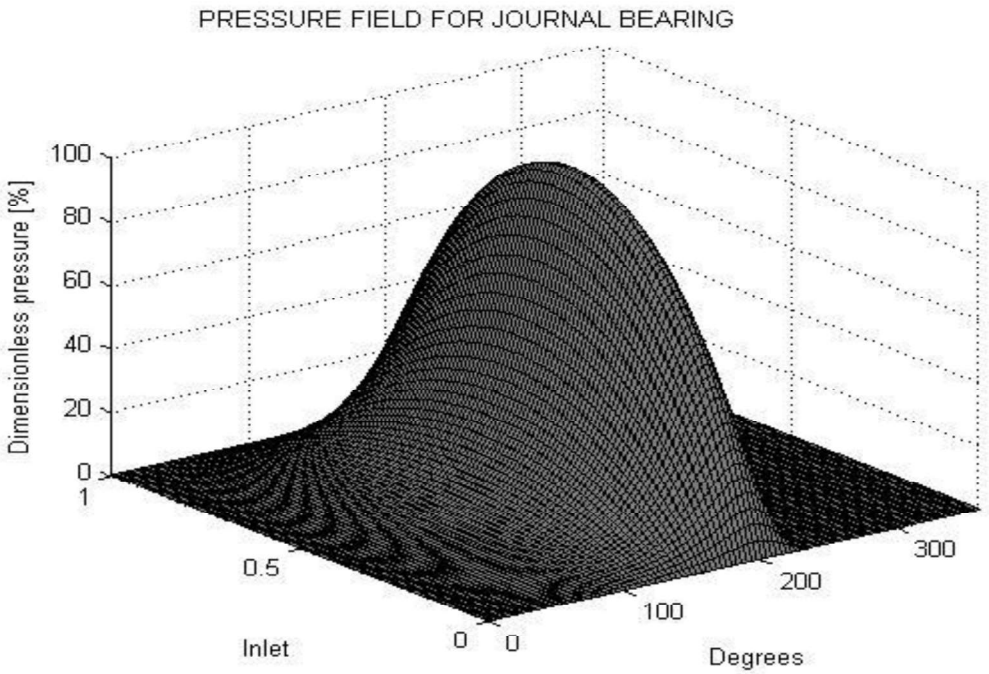

Figure 5.9 Pressure field for ε=0.7 and t=0

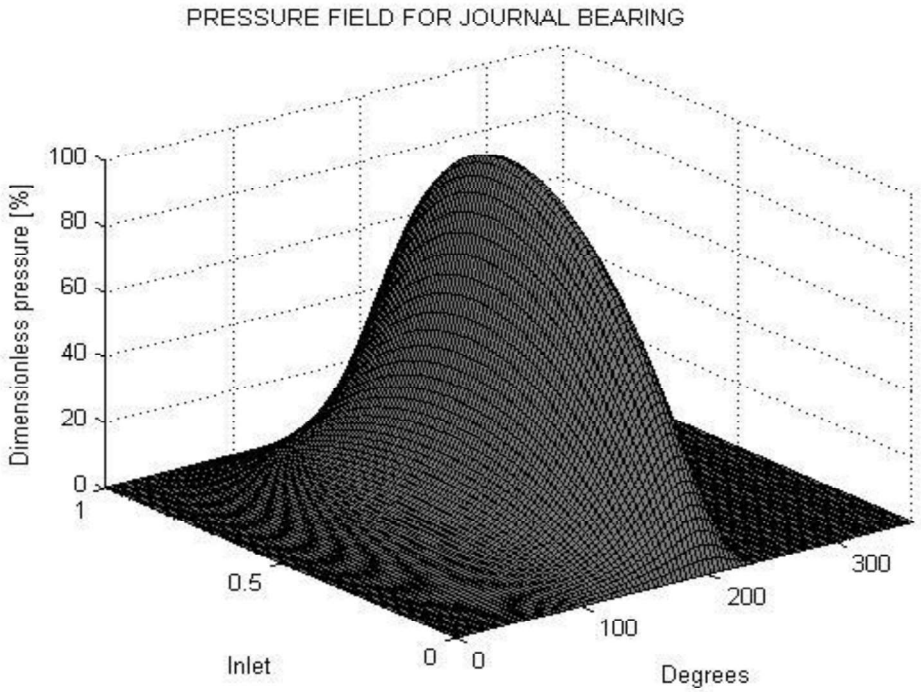

Figure 5.10 Pressure field for ε=0.7 and t=0.1

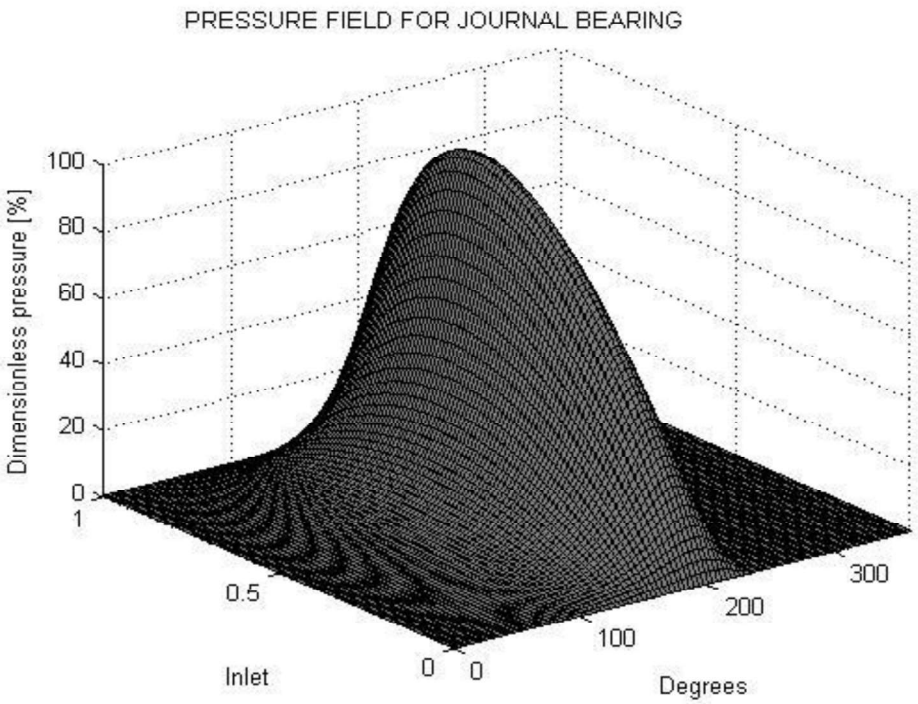

Figure 5.11 Pressure field for ε=0.7 and t=0.2

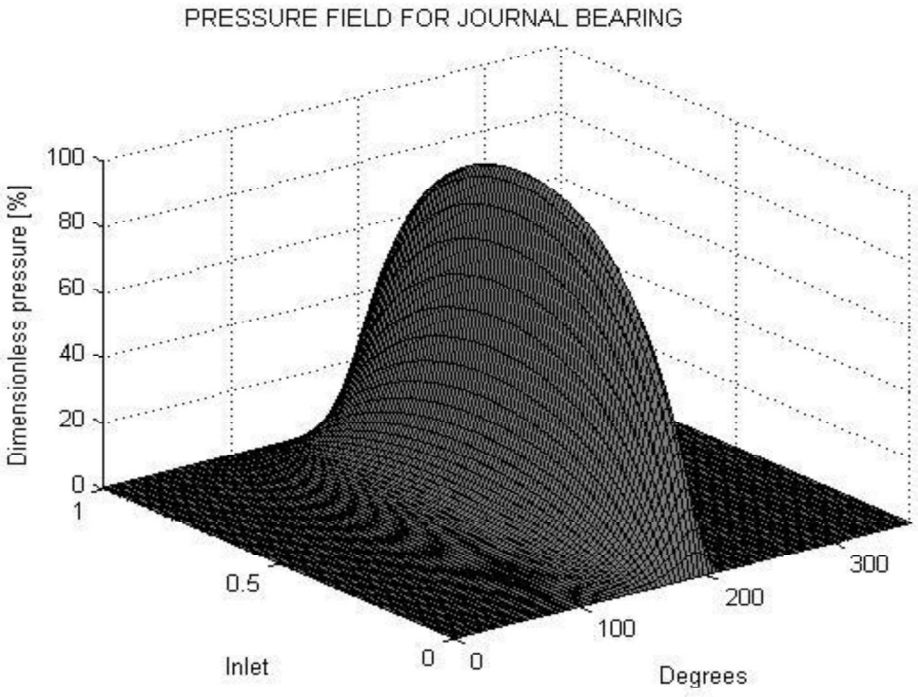

Figure 5.12 Pressure field for ε=0.9 and t=0

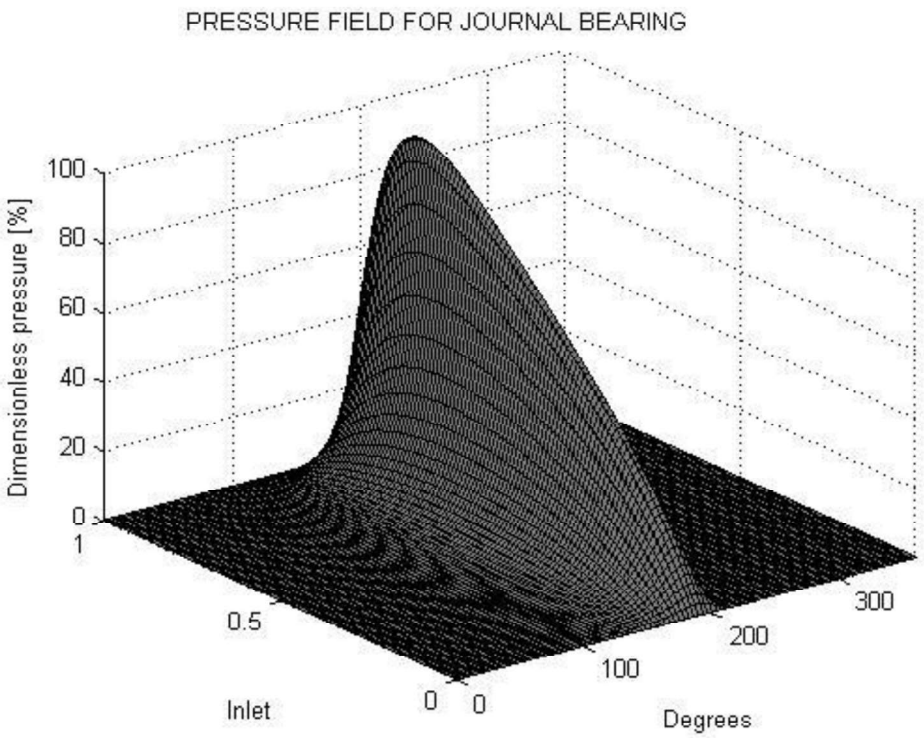

Figure 5.13 Pressure field for ε=0.9 and t=0.1

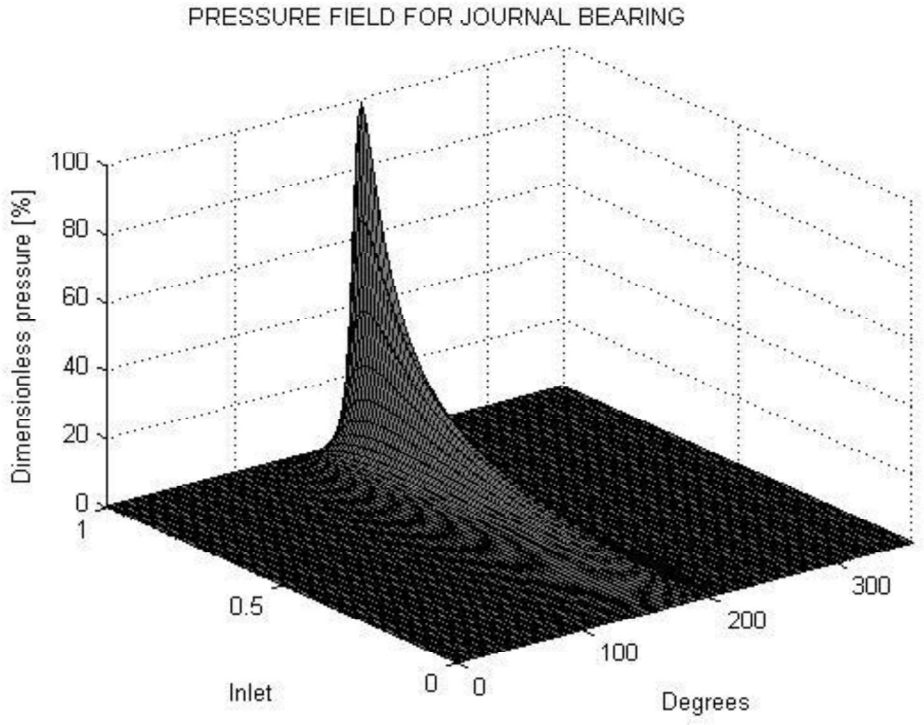

Figure 5.14 Pressure field for ε=0.9 and t=0.2

From the pressure fields depicted above, it can be seen that the peak pressure in shifting from middle in case of aligned bearing towards the end in the case of misaligned bearing. The shifting increases as the misalignment increases and the effect are more prominent at higher eccentricity ratios.

Computer program STABILITY was used to find out the variation in stiffness and damping coefficients due to misalignment. The characteristics of the bearing were calculated for a full journal bearing with different eccentricity ratios considering and without considering the misalignment effect. Misalignment parameter has been varied from 0 to 0.2 for the analysis of misaligned journal bearing. The results obtained have been discussed further.

The bearing model and lubricant specifications are same as in the previous iterations (table 5.1). An additional input of dimensionless mass was required, which was assumed to be constant (0.1) throughout the program. The iterations were carried out with 100 nodes in both x and y directions. The terminating value for residual for iterations to solve Vogelpohl equation and attitude angle were set to 0.000001 and 0.0001 respectively. The relaxation factors for both the iterations were set to 1.2 and 1 respectively. The maximum number cycles for both the iterations are limited to 100. The incremental displacement in x and y direction is 0.001 each and the incremental squeeze velocity is also take as 0.001 each.

S.No.	Eccentricity Ratio	Dimensionless critical frequency for misalignment parameter t=0	Dimensionless critical frequency for misalignment parameter t=0.1	Dimensionless critical frequency for misalignment parameter t=0.2
1.	0.1	2.4809	2.5404	2.6053
2.	0.3	2.8309	2.8344	2.8359
3.	0.5	3.524	3.9064	3.4592
4.	0.7	1.1822	1.1812	1.1602
5.	0.9	0.4549	0.41714	0.19715

Table 5.6 Variation in dimensionless critical frequency for different eccentricity ratios

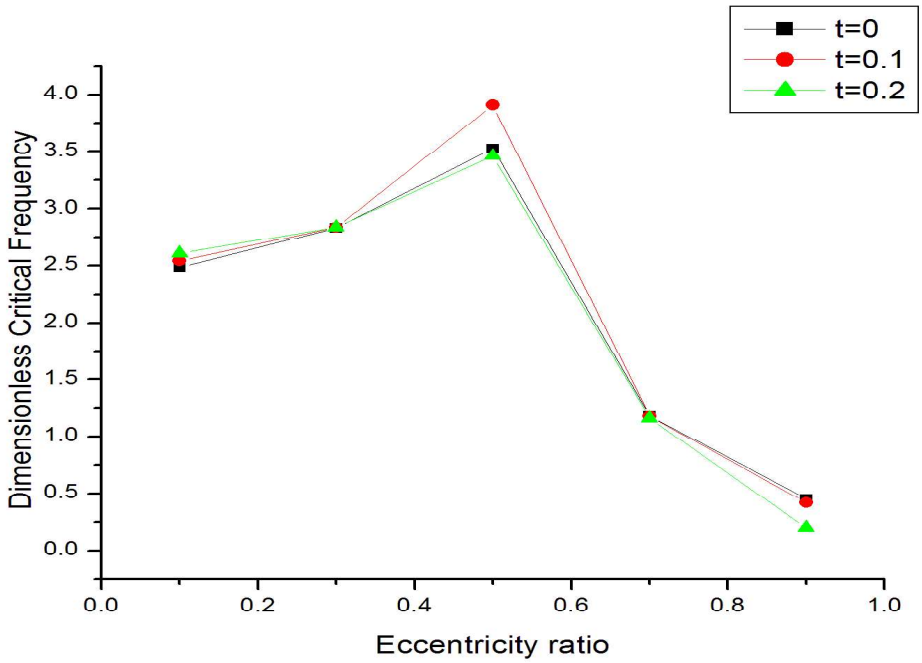

Figure 5.15 Graph for the variation in critical frequency

It has been found that the critical frequency decreases with the increase in misalignment. Thus, misaligned bearings must not be operated in close speeds to the critical speed as it may result in failure. However, at high values of misalignment, critical speed increases because of increase in k_{xx}.

S.No.	Eccentricity Ratio	Dimensionless stiffness coefficient for misalignment parameter t=0		Dimensionless stiffness coefficient for misalignment parameter t=0.1		Dimensionless stiffness coefficient for misalignment parameter t=0.2	
		k_{xx}	k_{xy}	k_{xx}	k_{xy}	k_{xx}	k_{xy}
1.	0.1	1.2652	1.8707	1.2253	1.7893	1.2971	1.8869
2.	0.3	1.4138	0.96116	1.4167	0.96263	1.4237	0.96403
3.	0.5	2.0101	1.3308	3.3929	3.8245	2.0283	1.3372
4.	0.7	3.1659	1.748	3.1931	1.7646	3.2885	1.8205
5.	0.9	10.055	4.578	11.615	5.1377	37.591	12.598

Table 5.7 Variation in dimensionless stiffness coefficient (in x dir.) for different eccentricity ratios

S.No.	Eccentricity Ratio	Dimensionless stiffness coefficient for misalignment parameter t=0		Dimensionless stiffness coefficient for misalignment parameter t=0.1		Dimensionless stiffness coefficient for misalignment parameter t=0.2	
		k_{yx}	k_{yy}	k_{yx}	k_{yy}	k_{yx}	k_{yy}
1.	0.1	-2.339	-0.68395	-2.2735	-0.53542	-2.2795	-0.4551
2.	0.3	-0.55014	0.61582	-0.54577	0.62262	-0.55566	0.62084
3.	0.5	0.08083	0.85868	-0.03005	0.91515	0.077504	0.8655
4.	0.7	0.33111	1.0963	0.33508	1.1009	0.3574	1.1182
5.	0.9	1.3237	1.6111	1.6142	1.7167	6.6052	2.7864

Table 5.8 Variation in dimensionless stiffness coefficient (in y dir.) for different eccentricity ratios

S.No.	Eccentricity Ratio	Dimensionless damping coefficient for misalignment parameter t=0		Dimensionless damping coefficient for misalignment parameter t=0.1		Dimensionless damping coefficient for misalignment parameter t=0.2	
		C_{xx}	C_{xy}	C_{xx}	C_{xy}	C_{xx}	C_{xy}
1.	0.1	4.9625	4.5134	4.8637	4.3367	5.0467	4.3748
2.	0.3	2.0616	2.217	2.0652	2.2155	2.0755	2.2139
3.	0.5	2.2227	2.5075	2.2304	6.6548	2.2369	2.5042
4.	0.7	2.7073	2.7069	2.7331	2.7209	2.8034	2.7409
5.	0.9	6.8445	4.2514	7.3814	4.223	12.363	4.3018

Table 5.9 Variation in dimensionless damping coefficients (in x dir.) for different eccentricity ratios

S.No.	Eccentricity Ratio	Dimensionless damping coefficient for misalignment parameter t=0		Dimensionless damping coefficient for misalignment parameter t=0.1		Dimensionless damping coefficient for misalignment parameter t=0.2	
		C_{yx}	C_{yy}	C_{yx}	C_{yy}	C_{yx}	C_{yy}
1.	0.1	-0.66668	4.0411	-0.50048	4.2757	-0.4919	4.4095
2.	0.3	0.4748	1.9749	0.4756	1.9626	0.46824	1.969
3.	0.5	0.73895	1.5216	0.765	1.5001	0.74304	1.5136
4.	0.7	1.1057	1.4349	1.1149	1.4393	1.1304	1.4265
5.	0.9	1.8652	1.2086	1.9241	1.1391	2.5728	0.90059

Table 5.10 Variation in dimensionless damping coefficients (in y dir.) for different eccentricity ratios

There is certain variation in the stiffness coefficients and the damping coefficients with the misalignment of shaft in a journal bearing. However, further analysis is required for the exact behaviour of a misaligned bearing in terms of stability conditions.

Chapter 6

Conclusions and further scope

Based on the results and discussions made in the previous chapter, following conclusions have been drawn for the configuration of bearing under study:

- The most observable effect of misalignment of bearing is the decrease in minimum film thickness. High values of misalignment may result in metal to metal contact.
- The maximum pressure increases in a misaligned bearing as compared to a perfectly aligned bearing. A large amount of increase in pressure is observed for high values of misalignment parameter.
- The maximum pressure acting in a perfectly aligned bearing is at the mid plane of the bearing. However, the position of maximum pressure gets shifted towards the end for a misaligned bearing.
- The coefficient of friction reduces considerably with increase in amount of misalignment in a journal bearing.
- The attitude angle gets reduced with increase in misalignment of a bearing.
- The critical frequency of bearing system is found to get reduced with increase in misalignment.
- There magnitude of stiffness and damping coefficients also changes due to misalignment.
- The results and conclusions discussed are found to be in much resemblance with the studies made earlier. The experimental results depicted by Bouyer et. al.[24] are found in agreement with the numerical results obtained from the Matlab program.

Numerical analysis of journal bearing was carried out in order to study the operating characteristics and stability parameters under the influence of misalignment. However, still many assumptions like constant viscosity of the lubricant, neglecting the negative pressures etc have been made during the analysis. The strong influence of secondary effects such as lubricant heating and bearing deformation on bearing parameters still need to be carried out. With increases in the speed of computing it may become possible to perform the simultaneous analysis of several different effects on bearing performance, e.g. the combined effect of heating,

deformation and misalignment. The finite difference method used in numerical analysis is versatile and simple to apply, but is also relatively inaccurate. Newer methods of devising numerical equivalents of differential equations are being increasingly adopted.

References

1. Gwidon W. Stachowiak, Andrew W. Batchelor; “Engineering Tribology”; Butterworth Heinemenn Publications; 1st edition, 1990
2. Hydrodynamic Bearings, by EPI Inc
3. Malcolm E. Leader; “Understanding Journal Bearings”; Applied Machinery Dynamics Co.; 2002
4. Reynolds, O.; “On the theory of lubrication and its application in Mr. Beaucamp Tower’s experiment"; Phil. Trans. of the Royal Society, London; 1886
5. Fisher, A.; “Oil Flow in Ring Lubricated Bearings”; Machinery, London, 21, pp. 311; 1922
6. McKee, S.A.; McKee, T.R.,; “Pressure distribution in the oil film of journal bearings”; Transactions of the ASME; 54:149-165; 1932
7. Piggott, R. J. S.; “Bearings and Lubrication. Bearing Troubles Traceable to Design can be Avoided by Engineering Study”, Mech. Eng. (American Society of Mechanical Engineers) 64, pp. 259–269; 1942
8. Dubois, G.B.; Ocvirk, F.W.; Wehe, R.L.; “Experimental Investigation of Oil Film Pressure Distribution for Misaligned Plain Bearings”; NCAC, Technical Note 2507, Washington; 1951
9. Dubois, G.B.; Ocvirk, F.W.; Wehe, R.L.; “Experimental Investigation of Misalignment Couples and Eccentricity at Ends of Misaligned Plain Bearings”; NCAC, Technical Note 3352, Washington; 1955
10. Dubois, G.B.; Ocvirk, F.W.; Wehe, R.L; “Properties of misaligned journal bearing”, Journal of Basic Engineering, 79:1205-1212; 1957
11. Smalley, A.J.; McCallion, H.,; “The Effect of Journal Misalignment on the Performance of a Journal Bearing Under Steady Running Conditions”; Proceedings of Institution of Mechanical Engineers, 181(Pt.3B):45-54; 1966
12. Asanable, S.; Akahoshi, M.; Asai, R.,; “Theoretical and experimental investigation of misaligned journal bearing performance”; Tribology Convention, Institution of Mechanical Engineers, London; C36/71; 1971

13. Pinkus, O.; Bupara, S.S.; “Analysis of misaligned grooved journal bearings”; Journal of Lubrication Technology, 101(4):503-509; 1979
14. Mokhtar, M.O.A.; Safar, Z.S.; Abd-EI-Rahman, M.A.M.; “An adiabatic solution of misalignment journal bearings”; ASME Journal of Lubrication Technology, 107(2):263-267; 1985
15. Buckholz, R.H.; Lin, J.F.; “The effect of journal bearing misalignment on load and cavitation for non-Newton lubricants”; Journal of Tribology, 108(4):645-654; 1986
16. Jiang, J.Y.; Chang, C.C; “Adiabatic solution for a misaligned journal bearing with non-Newtonian lubricants”; Tribology International, 20(5):267-275; 1987
17. Vijayaraghavan, D.; Keith, T.G.,; “Analysis of a finite misaligned journal bearing considering cavitation and starvation effects”; Journal of Tribology, 112(1):60-67; 1990
18. Bou-Said, B.; Nicolas, D.; “Effects of misalignment on static and dynamic characteristics of hybrid bearings”; Tribology Transactions, 35(2):325-331; 1992
19. Qiu, Z.L.; Tieu, A.K; “Misalignment effect on the static and dynamic characteristics of hydrodynamic journal bearings”; Journal of Tribology, 117(4):717-723; 1995
20. Qiu, Z.L.; Tieu, A.K; “Experimental study of freely alignable part 2: journal bearings dynamic characteristics”; Journal of Tribology, 118(3):503-508; 1996
21. Arumugam, P.; Swarnamani, S.; Prabhu, B.S.; “Effects of journal misalignment on the performance characteristics of three-lobe bearings”; Wear, 206(1-2):122-129; 1997
22. Banwait, S.S.; Chandrawat, H.N.; Adithan, M.,; “Thermo-hydrodynamic Analysis of Misaligned Plain Journal Bearing”; Proceeding of First Asia International Conference on Tribology, Beijing, p.35-40; 1998
23. Guha, S.K.; “Analysis of steady-state characteristics of misaligned hydrodynamic journal bearings with isotropic roughness effect”; Tribology International, 33(1):1-12; 2000
24. Bouyer, J.; Fillon, M.; “An experimental analysis of misalignment effects on hydrodynamic plain journal bearing performances”; Journal of Tribology, 124(2): 313-319; 2002
25. Pierre, I.; Bouyer, J.; Fillon, M.; “Thermo-hydrodynamic behavior of misaligned plain journal bearings: theoretical and experimental approaches”; Tribology Transactions, 47(4):594-604; 2004

26. Boedo, S.; Booker, J.F.,; “Classic bearing misalignment and edge loading: a numerical study of limiting cases”; Journal of Tribology, 126(3):535-541; 2004
27. Ma, Y.Y.; “Performance of dynamically loaded journal bearings lubricated with couple stress fluids considering the elasticity of the liner”; Journal of Zhejiang University-SCIENCE A (Applied Physics & Engineering), 9(7): 916-921; 2008
28. Sun, J.; Deng, M.; Fu, Y.H.; Gui, C.L.; “Thermo-hydrodynamic lubrication analysis of misaligned plain journal bearing with rough surface”; Journal of Tribology, 132(1):011704; 2010
29. Wang et al.; “A mixed-TEHD analysis and experiment of journal bearings under severe operating conditions”; Tribology International 35 pp. 395–407; 2002
30. Jang, J.Y.; Khonsari, M.M.; "On the behavior of misaligned journal bearings based on mass-conservative thermo-hydrodynamic analysis”; Journal of Tribology, 132(1):011702; 2010
31. A.M. El-Butch, N.M. Ashour; “Transient analysis of misaligned elastic tilting-pad journal bearing”; Tribology International 38 p41–48; 2005
32. Das A.K, ; “On the steady-state performance of misaligned hydrodynamic journal bearings lubricated with micro-polar fluids”; Tribology International 35:201–10; 2002
33. Padelis G. Nikolakopoulos, Chris A. Papadopoulos; “A study of friction in worn misaligned journal bearings under severe hydrodynamic lubrication”; Elsevier Tribology International vol41, pp461–472; 2010
34. Satish B. Shenoy, R. Pai ; “Theoretical investigations on the performance of an externally adjustable fluid-film bearing including misalignment and turbulence effects”; Tribology International 42, pp1088–1100; 2009
35. Jun Sun, Gui Changlin; “Hydrodynamic lubrication analysis of journal bearing considering misalignment caused by shaft deformation”; Tribology International 37, pp841–848; 2004
36. Jun Sun, Changlin Gui, Zhiyuan Li; “An experimental study of journal bearing lubrication effected by journal misalignment as a result of shaft deformation under load”; Journal of Tribology, Vol. 127; pp813-819; 2005
37. Guohui Xu; Jian Zhou; Haipeng Geng; Mingjian Lu; Lihua Yang; Lie Yu; “Research on the static and dynamic characteristics of misaligned journal bearing considering the

turbulent and thermo-hydrodynamic effects"; Journal of Tribology, Vol. 137, pp024504/1-8; 2015

38. Joon Young Jang, Michael M. Khonsari; "Review on the characteristics of misaligned journal bearings"; Lubricants 3, pp27-53; 2015
39. J.A. Tichy and S.H. Chen; "Plane Slider Bearing Load Due to Fluid Inertia - Experiment and Theory"; Transactions ASME, Journal of Lubrication Technology, Vol. 107, pp. 32-38; 1987
40. H.I. You and S.S. Lu; "Inertia Effect in Hydrodynamic Lubrication With Film Rupture, Transactions ASME", Journal of Tribology, Vol. 109, pp. 87-90; 1987.
41. H.I. You and S.S. Lu; "The Effect of Fluid Inertia on the Operating Characteristics of a Journal Bearing", Transactions ASME, Journal of Tribology, Vol. 110, pp. 499-502, 1988
42. G. Vogelpohl, "Beitrage zur Kenntnis der Gleitlagerreibung", Ver. Deutsch. Ing., Forschungsheft, pp. 386;1937
43. M.M. Reddi and T.Y. Chu; "Finite element solution of the steady-state incompressible lubrication problem"; Transactions ASME, Journal of Lubrication Technology, Vol. 92, pp. 495-503; 1970.
44. J.F. Booker and K.K. Huebner, "Application of finite element methods to lubrication, an engineering approach", Transactions ASME, Journal of Lubrication Technology, Vol. 94,pp. 313-323; 1972
45. A. Cameron, Principles of Lubrication, Chapter by M.R. Osborne on Computation of Reynolds' Equation, Longmans, London, pp. 426-439; 1966
46. D. Dowson, A.A.S. Miranda and C.M. Taylor, Implementation of an Algorithm Enabling the Determination of Film Rupture and Reformation Boundaries in a Liquid Film Bearing, Proc. 10th Leeds-Lyon Symposium; pp. 60-70; 1984
47. T. Someya, Journal-Bearing Data-Book, Springer Verlag, Berlin, Heidelberg, 1989
48. A.J. Colynuck and J.B. Medley, "Comparison of two finite difference methods for the numerical analysis of thermohydrodynamic lubrication", Tribology Transactions, Vol. 32, pp. 346-356;1989

Appendix

Program MISALIGNMENT

```
clc; cla reset; echo off;
global tbv tbs tbp tbt tbd tbg tba tbinfo tbclose;
set([tbv tbs tbt tbd tbg tba tbinfo tbclose],'Enable','off');
% BEGIN OF INPUT DATA
% -------------------
prompt = {'Eccentricity ratio:', 'L/D ratio:', 'Arc bearing angle [°]:',
'Misaligment parameter from interval [0,0.5]:'};
title='INPUT DATA (PARTIAL)'; lineno=1; def={'0.8','1', '120', '0'}; answer=
inputdlg(prompt,title,lineno,def);
if size(answer) == 0, % PROGRAM IS TERMINATED
    set(tbp, 'Value', get(tbp, 'Min')); set([tbv tbs tbt tbd tbg tba tbinfo
tbclose],'Enable','on'); break; end;
[epsilon,loverd,alpha,t] = deal(answer{:}); epsilon = str2num(epsilon);
loverd = str2num(loverd);
alpha = str2num(alpha); t = str2num(t); slender = 0.5/loverd; alpha =
alpha*pi/180;
if t < 0, t = 0; end; if t > 0.5, t = 0.5; end;
% SET MESH CONSTANTS
prompt = {'Number of nodes in the i or x direction:','Number of nodes in the
j or y direction:','Terminating value of residual for iter. to solve
Vogelpohl equation:','Terminating value of residual for iter. to find
attitude angle:','Relaxation factor of iter. to solve Vogelpohl
equation:','Relaxation factor of iter. to find attitude angle:','Max number
of cycles during iter. to solve Vogelpohl equation:','Max number of cycles
during iter. to find attitude angle:'};
title='INPUT DATA (PARTIAL)'; lineno=1; def={'11','11','0.000001', '0.0001',
'1.2', '1', '100','30'};
answer= inputdlg(prompt,title,lineno,def);
if size(answer) == 0, % PROGRAM IS TERMINATED
    set(tbp, 'Value', get(tbp, 'Min')); set([tbv tbs tbt tbd tbg tba tbinfo
tbclose],'Enable','on'); break; end;
[inode,jnode,reslim1,reslim2,factor1,factor2,nlim1,nlim2] = deal(answer{:});
inode = str2num(inode); jnode = str2num(jnode); reslim1 = str2num(reslim1);
reslim2 = str2num(reslim2);
factor1 = str2num(factor1); factor2 = str2num(factor2); nlim1 =
str2num(nlim1); nlim2 = str2num(nlim2);
% END OF INPUT DATA
% -----------------
subplot(1,1,1);
text('units','normalized','position',[0.2 0.55], 'FontWeight',
'bold','color',[1 0 0], 'string', 'CALCULATIONS IN PROGRESS');
figure(1); slender = 0.5/loverd; deltax = alpha/(inode-1); deltay = 1/(jnode-
1);
% DIFFERENTIAL QUANTITIES FOR STABILITy CALCULATIONS
% INITIALIZE VALUES OF M(I,J), SWITCH(I,J) AND P(I,J)
M = zeros(inode,jnode); P = zeros(inode,jnode);
% SET INITIAL VALUE OF OFFSET ANGLE
beta = 0;
% ENTER ATTITUDE ANGLE ITERATION CYCLE, CALCULATE H, F AND G VALUES
n2 = 0; betas = 0; residb = reslim2 + 10;
while (residb > reslim2) & (n2 < nlim2),
    n2 = n2 + 1;
```

```
    for i = 1:inode,
        xaux = (i-1)*deltax + pi - 0.5*alpha; theta = xaux - beta;
        for j = 1:jnode,
            y = (j-1)*deltay - 0.5; h0 = y*t*cos(xaux) + epsilon*cos(theta) +
1;
            dhdx0 = -y*t*sin(xaux) - epsilon*sin(theta); d2hdx20 = -
y*t*cos(xaux) - epsilon*cos(theta);
            dhdy0 = t*cos(xaux); d2hdy20 = 0; H(i,j) = h0; G(i,j) =
dhdx0/h0^1.5;
            F(i,j) = 0.75*(dhdx0^2 + (slender*dhdy0)^2)/h0^2 + 1.5*(d2hdx20 +
d2hdy20*slender^2)/h0;
        end;
    end;
    coeff1 = 1/deltax^2; coeff2 = (slender/deltay)^2;
    % ----------------------------------------
    % SUBROUTINE TO SOLVE THE VOGELPOHL EQUATION
    sum2 = 0; n1 = 0; residp = reslim1 + 10;
    while (residp > reslim1) & (n1 < nlim1),
        n1 = n1 + 1; sum = 0;
        for i = 2:inode-1,
            for j = 2:jnode-1,
                store = ((M(i+1,j) + M(i-1,j))*coeff1 + (M(i,j+1) + M(i,j-
1))*coeff2 -G(i,j))/(2*coeff1 + 2*coeff2 + F(i,j));
                M(i,j) = M(i,j) + factor1*(store-M(i,j));
                if M(i,j) < 0, M(i,j) = 0; end;
                sum = sum + M(i,j);
            end;
        end;
        residp = abs((sum-sum2)/sum); sum2 = sum;
    end;
    % ----------------------------------------
    % FIND PRESSURE FIELD FROM VOGELPOHL PARAMETER
    for i = 2:inode-1,
        for j = 2:jnode-1,
            P(i,j) = M(i,j)/H(i,j)^1.5;
        end;
    end;
    % ITERATION RESIDUAL ON ATTITUDE ANGLE ITERATION
    % CALCULATE TRANSVERSE AND AXIAL LOADS
    % ----------------------------------
    % SUBROUTINE TO INTERGRATE FOR FORCES
    for i = 1:inode,
        SUMY(i) = 0;
        for j = 2:jnode, SUMY(i) = SUMY(i) + P(i,j) + P(i,j-1); end;
        SUMY(i) = SUMY(i)*0.5*deltay;
    end;
    axialw = 0; transw = 0;
    for i = 2:inode,
        x = (i-1)*deltax + pi - 0.5*alpha; x2 = (i-2)*deltax + pi -
0.5*alpha;
        axialw = axialw - cos(x)*SUMY(i) - cos(x2)*SUMY(i-1); transw = transw
+ sin(x)*SUMY(i) + sin(x2)*SUMY(i-1);
    end;
    axialw = axialw*deltax*0.5; transw = transw*deltax*0.5;
    % ------------------------
    loadw = sqrt(axialw^2 + transw^2); attang = atan(transw/axialw);
```

```
    if axialw > 0, attang1 = attang; end; if axialw < 0, attang1 = -attang;
end;
    beta = beta + factor2*attang1; residb = abs((beta-betas)/beta); betas =
beta;
end;
% ----------------------------------------
for j = 1:jnode, ICAV(j) = 1000; end;
for j = 2:jnode-1,
    for i = 2:inode,
        if (M(i,j) == 0) & (ICAV(j) == 1000), ICAV(j) = i; end;
    end;
end
% EXTRAPOLATED VALUES OF ICAV(J) AT EDGES OF BEARING
ICAV(1) = 2*ICAV(2) - ICAV(3); if ICAV(1) < 1, ICAV(1) = 1; end;
if ICAV(1) > inode, ICAV(1) = inode; end; ICAV(jnode) = 2*ICAV(jnode-1) -
ICAV(jnode-2);
if ICAV(jnode) < 1, ICAV(jnode) = 1; end; if ICAV(jnode) > inode, ICAV(jnode)
= inode; end;
% CALCULATE FRICTION COEFFICIENT
% FIND VALUES OF DIMENSIONLESS SHEAR STRESS
for i = 1:inode,
    for j = 1:jnode,
        % CALCULATE dpdx FROM DOWNSTREAM VALUES
        if i > 1, dpdx = (P(i,j) - P(i-1,j))/deltax; end;
        % VALUE OF dpdx FOR i = 1
        if i == 1, dpdx = P(2,j)/deltax; end; if i < ICAV(j), TORR(i,j) =
1/H(i,j) + 3*dpdx*H(i,j); end;
        if i == ICAV(j), TORR(i,j) = 1/H(i,j); end; i10 = ICAV(j);
        if i > ICAV(j), TORR(i,j) = H(i10,j)/H(i,j)^2; end;
    end;
end;
% INTEGRATE FOR TORR(i,j) OVER X AND Y
for i = 1:inode,
    % LINE INTEGRAL IN Y-SENSE
    SUMY(i) = 0;
    for j = 2:jnode, SUMY(i) = SUMY(i) + TORR(i,j) + TORR(i,j-1); end;
    SUMY(i) = SUMY(i)*0.5*deltay;
end;
friction = 0;
for i = 2:inode, friction = friction + SUMY(i) + SUMY(i-1); end;
friction = friction*0.5*deltax;
% ----------------------------
% CALCULATE DIMENSIONLESS FRICTION COEFFICIENT
myu = friction/loadw;
% SEARCH FOR MAXIMUM PRESSURE
pmax = 0;
for i = 2:inode-1,
    for j = 2:jnode-1,
        if P(i,j) > pmax, pmax = P(i,j); end;
    end;
end;
% EXPRESS ALL PRESSURES AS PERCENTAGE OF MAXIMUM PRESSURE
for i = 1:inode,
    for j = 1:jnode,
        P(i,j) = P(i,j)*100/pmax;
    end;
end;
```

```
% PRESSURE FIELD PLOT
xi = 0:inode-1; yj = 0:jnode-1; xi = (xi*alpha*180/pi)/(inode-1); yj =
yj/(jnode-1);
colormap([0.5 0.5 0.5]); subplot(1,1,1); surfl(xi,yj,P'); axis([0 max(xi) 0 1
0 100]);
xlabel('Degrees'); ylabel('Inlet'); zlabel('Dimensionless pressure [%]');
text('units','normalized','position',[0.1 1.05],'string', 'PRESSURE FIELD FOR
JOURNAL BEARING');
% PRINT OUT VALUES OF INPUT AND OUTPUT DATA
% ----------------------------------------
fprintf(' \n'); fprintf(' INPUT AND OUTPUT DATA FOR PROGRAM PARTIAL\n');
fprintf(' \n');
fprintf(' INPUT DATA:\n');
fprintf(' Eccentricity ratio = %0.5g\n',epsilon);
fprintf(' L/D ratio = %0.5g\n',loverd);
fprintf(' Bearing arc angle = %0.5g°\n',alpha*180/pi);
fprintf(' Misaligment parameter = %0.5g\n',t);
fprintf(' \n');
fprintf(' OUTPUT DATA:\n');
fprintf(' Dimensionless load = %0.5g\n', loadw);
fprintf(' Attitude angle = %0.5g°\n',beta*180/pi);
fprintf(' Dimensionless friction coefficient = %0.5g\n', myu)
fprintf(' Maximum dimensionless pressure = %0.5g\n',pmax);
fprintf(' \n'); fprintf(' PROGRAM MISALIGNMENT HAS BEEN COMPLETED\n');
set(tbp, 'Value', get(tbp, 'Min')); set([tbv tbs tbt tbd tbg tba tbinfo
tbclose],'Enable','on');
```

Program STABILITY

```
clc; cla reset; echo off; warning off;
global reslim1 nlim1 inode jnode SWITCH1 M G F coeff1 coeff2 sum2;
global SUMY P deltay deltax axialw transw alpha factor1 residp;
clear global reslim1 nlim1 inode jnode SWITCH1 M G F coeff1 coeff2 sum2;
clear global SUMY P deltay deltax axialw transw alpha factor1 residp;
global tbv tbs tbp tbt tbd tbg tba tbinfo tbclose;
set([tbv tbs tbp tbt tbd tbg tbinfo tbclose],'Enable','off');
% BEGIN OF INPUT DATA
% -------------------
prompt = {'Eccentricity ratio:','L/D ratio:','Arc bearing angle
[°]:','Misaligment parameter from interval [0,0.5]:','Dimensionless exciter
mass:'};
title='INPUT DATA (STABILITY)'; lineno=1; def={'0.7', '1', '120',
'0.3','0.1'}; answer= inputdlg(prompt,title,lineno,def);
if size(answer) == 0, % PROGRAM IS TERMINATED
    set(tba, 'Value', get(tba, 'Min')); set([tbv tbs tbp tbt tbd tbg tbinfo
tbclose],'Enable','on'); break; end;
[epsilon,loverd,alpha,t,gamma] = deal(answer{:}); epsilon = str2num(epsilon);
loverd = str2num(loverd);
alpha = str2num(alpha); t = str2num(t); gamma = str2num(gamma); alpha =
alpha*pi/180;
prompt = {'Number of nodes in the i or x direction:','Number of nodes in the
j or y direction:','Terminating value of residual for iter. to solve
Vogelpohl equation:','Terminating value of residual for iter. to find
attitude angle:','Relaxation factor of iter. to solve Vogelpohl
equation:','Relaxation factor of iter. to find attitude angle:'};
```

```
title='INPUT DATA (STABILITY)'; lineno=1; def={'11', '11', '0.0000001',
'0.00001', '1.2','1'};
answer= inputdlg(prompt,title,lineno,def);
if size(answer) == 0, % PROGRAM IS TERMINATED
    set(tba, 'Value', get(tba, 'Min')); set([tbv tbs tbp tbt tbd tbg tbinfo
tbclose],'Enable','on'); break; end;
[inode,jnode,reslim1,reslim2,factor1,factor2] = deal(answer{:}); inode =
str2num(inode); jnode = str2num(jnode);
reslim1 = str2num(reslim1); reslim2 = str2num(reslim2); factor1 =
str2num(factor1); factor2 = str2num(factor2);
prompt = {'Max number of cycles during iter. to solve Vogelpohl
equation:','Max number of cycles during iter. to find attitude
angle:','Incremental displacement in x direction:','Incremental displacement
in y direction:','Incremental squeeze velocity in x direction of the above
axes:','Incremental squeeze velocity in y direction of the above axes:'};
title='INPUT DATA (STABILITY)'; lineno=1;
def={'100','30','0.001','0.001','0.001','0.001'};
answer= inputdlg(prompt,title,lineno,def);
if size(answer) == 0, % PROGRAM IS TERMINATED
    set(tba, 'Value', get(tba, 'Min')); set([tbv tbs tbp tbt tbd tbg tbinfo
tbclose],'Enable','on'); break; end;
[nlim1,nlim2,dx,dy,w0x,w0y] = deal(answer{:}); nlim1 = str2num(nlim1); nlim2
= str2num(nlim2);
dx = str2num(dx); dy = str2num(dy); w0x = str2num(w0x); w0y = str2num(w0y);
% END OF INPUT DATA]
% -----------------
subplot(1,1,1);
text('units','normalized','position',[0.2 0.55], 'FontWeight',
'bold','color',[1 0 0], 'string', 'CALCULATIONS IN PROGRESS');
figure(1); deltax = alpha/(inode-1); deltay = 1/(jnode-1); slender =
0.5/loverd;
% INITIALIZE VALUES OF M(i,j), SWITCH1(i,j) & P(i,j)
M = zeros(inode,jnode); SWITCH1 = zeros(inode,jnode); P = zeros(inode,jnode);
% SET INITIAL VALUE OF OFFSET ANGLE
beta = 0;
% ENTER ATTITUDE ANGLE ITERATION CYCLE, CALCULATE H,F & G VALUES
n2 = 0; betas = 0; residb = reslim2 + 10;
while (residb > reslim2) & (n2 < nlim2),
    n2 = n2+1;
    for i = 1:inode,
        x = (i-1)*deltax + pi - 0.5*alpha; theta = x - beta;
        for j = 1:jnode,
            y = (j-1)*deltay - 0.5; h0 = y*t*cos(x) + epsilon *cos(theta) +
1; dhdx0 = -y*t*sin(x) - epsilon *sin(theta);
            d2hdx20 = -y*t*cos(x) - epsilon *cos(theta); dhdy0 = t*cos(x);
d2hdy20 = 0; H(i,j) = h0; G(i,j) = dhdx0/h0^1.5;
            F(i,j) = 0.75*(dhdx0^2 + (slender*dhdy0)^2)/h0^2 + 1.5*(d2hdx20 +
d2hdy20*slender^2)/h0;
            DHDX(i,j) = dhdx0; D2HDX2(i,j) = d2hdx20; DHDY(i,j) = dhdy0;
        end;
    end;
    coeff1 = 1/deltax^2; coeff2 = (slender/deltay)^2;
    % SUBROUTINE TO SOLVE THE VOGELPOHL EQUATION
    vogel_stability;
    % FIND PRESSURE FIELD FROM VOGELPOHL PARAMETER
    for i = 2:inode-1,
        for j = 2:jnode-1,
```

```
            P(i,j) = M(i,j)/H(i,j)^1.5;
        end;
    end;
    % ITERATION RESIDUAL ON ATTITUDE ANGLE ITERATION
    % SUBROUTINE TO CALCULATE TRANSVERSE AND AXIAL LOADS
    loads_stability;
    loadw = sqrt(axialw^2 + transw^2); attang = atan(transw/axialw);
    if axialw > 0, attang1 = attang; end; if axialw < 0, attang1 = -attang;
end;
    beta = beta + factor2*attang1; residb = abs((beta-betas)/beta); betas =
beta;
end;
% STABILIZATION OF M(i,j) FIELD BEFORE COMPUTATION OF STIFFNESS AND
% DAMPING COEFFICIENTS *** FIX LOCATION OF CAVITATION FRONT USING
SWITCH1(i,j)
for i = 2:inode-1,
    for j = 2:jnode-1,
        if M(i,j) == 0, SWITCH1(i,j) = 1; end;
    end;
end;
% CALCULATE VALUES OF F(i,j) AND G(i,j) USING FINAL VALUE OF beta
for i = 1:inode,
    x = (i-1)*deltax + pi - 0.5*alpha; theta = x - beta;
    for j = 1:jnode,
        y = (j-1)*deltay - 0.5; h0 = y*t*cos(x) + epsilon *cos(theta) + 1;
dhdx0 = -y*t*sin(x) - epsilon *sin(theta);
        d2hdx20 = -y*t*cos(x) - epsilon *cos(theta); dhdy0 = t*cos(x);
d2hdy20 = 0; H(i,j) = h0; G(i,j) = dhdx0/h0^1.5;
        F(i,j) = 0.75*(dhdx0^2 + (slender*dhdy0)^2)/h0^2 + 1.5*(d2hdx20 +
d2hdy20*slender^2)/h0;
        DHDX(i,j) = dhdx0; D2HDX2(i,j) = d2hdx20; DHDY(i,j) = dhdy0;
    end;
end;
% RE-ITERATE: REMOVE ANY CAVITATION INDUCED INSTABILITIES IN M FIELD
% SUBROUTINE TO SOLVE THE VOGELPOHL EQUATION
vogel_stability;
% SAVE VALUES OF M(i,j)
for i = 1:inode,
    for j = 1:jnode,
        MSAVE(i,j) = M(i,j);
    end;
end;
% SUBROUTINE TO CALCULATE TRANSVERSE AND AXIAL LOADS
loads_stability; loadw = sqrt(axialw^2 + transw^2); loadw1 = loadw;
% CALCULATE STIFFNESS COEFFICIENTS kxx AND kyx
for i = 1:inode,
    x = (i-1)*deltax + pi -0.5*alpha;
    for j = 1:jnode,
        h0 = H(i,j) + dx*cos(x); dhdx0 = DHDX(i,j) - dx*sin(x); d2hdx20 =
D2HDX2(i,j) - dx*cos(x); G(i,j) = dhdx0/h0^1.5;
        F(i,j) = 0.75*(dhdx0^2 + (slender*DHDY(i,j))^2)/h0^2 +
1.5*d2hdx20/h0;
    end;
end;
% SUBROUTINE TO SOLVE THE VOGELPOHL EQUATION
vogel_stability;
% CALCULATE CHANGE IN FORCES
```

```
for i = 1:inode,
    x = (i-1)*deltax + pi - 0.5*alpha;
    for j = 1:jnode,
        P(i,j) = M(i,j)/(H(i,j)+dx*cos(x))^1.5- MSAVE(i,j)/H(i,j)^1.5;
    end;
end;
% SUBROUTINE TO CALCULATE TRANSVERSE AND AXIAL LOADS
loads_stability; kxx = axialw/(dx*loadw1); kyx = -transw/(dx*loadw1);%
CALCULATE STIFFNESS COEFFICIENTS kxx AND kyx
for i = 1:inode,
    x = (i-1)*deltax + pi - 0.5*alpha;
    for j = 1:jnode,
        h0 = H(i,j) + dy*sin(x); dhdx0 = DHDX(i,j) + dy*cos(x); d2hdx20 =
D2HDX2(i,j) - dy*sin(x); G(i,j) = dhdx0/h0^1.5;
        F(i,j) = 0.75*(dhdx0^2 + (slender*DHDY(i,j))^2)/h0^2 +
1.5*d2hdx20/h0;
    end;
end;
% SUBROUTINE TO SOLVE THE VOGELPOHL EQUATION
vogel_stability;
% CALCULATE CHANGE IN FORCES
for i = 1:inode
    x = (i-1)*deltax + pi - 0.5*alpha;
    for j = 1:jnode, P(i,j) = M(i,j)/(H(i,j)+dy*sin(x))^1.5 -
MSAVE(i,j)/H(i,j)^1.5; end;
end;
% SUBROUTINE TO CALCULATE TRANSVERSE AND AXIAL LOADS
loads_stability; kyy = -transw/(dy*loadw1); kxy = axialw/(dy*loadw1);
% CALCULATE DAMPING FORCES cxx AND cyx
for i = 1:inode,
    x = (i-1)*deltax + pi - 0.5*alpha; w = w0x*cos(x);
    for j = 1:jnode,
        G(i,j) = (DHDX(i,j) + 2*w)/H(i,j)^1.5;
        F(i,j) = 0.75*(DHDX(i,j)^2 + (slender*DHDY(i,j))^2)/H(i,j)^2 +
1.5*D2HDX2(i,j)/H(i,j);
    end;
end;
% SUBROUTINE TO SOLVE THE VOGELPOHL EQUATION
vogel_stability;
% CALCULATE CHANGE IN FORCES
for i = 1:inode,
    for j = 1:jnode, P(i,j) = M(i,j)/H(i,j)^1.5 - MSAVE(i,j)/H(i,j)^1.5; end;
end;
% SUBROUTINE TO CALCULATE TRANSVERSE AND AXIAL LOADS
loads_stability;
% CALCULATE DAMPING FORCES cxx AND cyx
cxx = axialw/(w0x*loadw1); cyx = -transw/(w0x*loadw1);
for i = 1:inode,
    x = (i-1)*deltax + pi - 0.5*alpha; w = w0y*sin(x);
    for j = 1:jnode,
        G(i,j) = (DHDX(i,j) + 2*w)/H(i,j)^1.5;
    end;
end;
% SUBROUTINE TO SOLVE THE VOGELPOHL EQUATION
vogel_stability;
% CALCULATE CHANGE IN FORCES
for i = 1:inode,
```